

Highlights

- First bromine partition experiments performed with natural silicate glasses
- First Br fluid/melt partition coefficients on mafic and intermediate compositions
- $D_{\text{Br}}^{f/m}$ increases with SiO_2 content of the melt, from basalt to rhyodacite compositions
- First Br data in melt inclusions from Etna, Stromboli, Merapi and Santorini volcanoes
- First model describing Br degassing behaviour in mafic volcanic systems

**The role of melt composition on aqueous fluid vs. silicate melt
partitioning of bromine in magmas**

Anita Cadoux^{a,b,c,d}, Giada Iacono-Marziano^{a,b,c}, Bruno Scaillet^{a,b,c}, Alessandro Aiuppa^{e,f},
Tamsin A. Mather^g, David M. Pyle^g, Etienne Deloule^h, Emanuela Gennaro^{a,b,c,f}, Antonio
Paonita^e

^a Université d'Orléans, ISTO, UMR 7327, 45071, Orléans, France

^b CNRS, ISTO, UMR 7327, 45071 Orléans, France

^c BRGM, ISTO, UMR 7327, BP 36009, 45060 Orléans, France

^d GEOPS, Univ. Paris-Sud, CNRS, Université Paris-Saclay, 91405 Orsay, France

^e Istituto Nazionale di Geofisica e Vulcanologia, Sezione di Palermo, Italy

^f DiSTeM, Università di Palermo, Italy

^g Department of Earth Science, University of Oxford, Oxford OX1 3AN, United Kingdom

^h CNRS, CRPG, Université de Lorraine, UMR 7358, BP 20, 54501 Vandoeuvre-lès-Nancy Cedex, France

Corresponding author: Anita Cadoux

E-mail: anita.cadoux@u-psud.fr

Revised manuscript for publication in *EPSL*

Abstract

Volcanogenic halogens, in particular bromine, potentially play an important role in the ozone depletion of the atmosphere. Understanding bromine behaviour in magmas is therefore crucial to properly evaluate the contribution of volcanic eruptions to atmospheric chemistry and their environmental impact. To date, bromine partitioning between silicate melts and the gas phase is very poorly constrained, with the only relevant experimental studies limited to investigation of synthetic melt with silicic compositions. In this study, fluid/melt partitioning experiments were performed using natural silicate glasses with mafic, intermediate and silicic compositions. For each composition, experiments were run with various Br contents in the initial fluid (H₂O-NaBr), at T - P conditions representative of shallow magmatic reservoirs in volcanic arc contexts (100-200 MPa, 900-1200°C). The resulting fluid/melt partition coefficients ($D_{\text{Br}}^{\text{f/m}}$) are: 5.0 ± 0.3 at 1200°C -100 MPa for the basalt, 9.1 ± 0.6 at 1060°C - 200 MPa for the andesite and 20.2 ± 1.2 at 900°C - 200 MPa for the rhyodacite. Our experiments show that $D_{\text{Br}}^{\text{f/m}}$ increases with increasing SiO₂ content of the melt (as for chlorine) and suggest that it is also sensitive to melt temperature (increase of $D_{\text{Br}}^{\text{f/m}}$ with decreasing temperature). We develop a simple model to predict the S-Cl-Br degassing behaviour in mafic systems, which accounts for the variability of S-Cl-Br compositions of volcanic gases from Etna and other mafic systems, and shows that coexisting magmatic gas and melt evolve from S-rich to Cl-Br enriched (relative to S) upon increasing degree of degassing. We also report first Br contents for melt inclusions from Etna, Stromboli, Merapi and Santorini eruptions and calculate the mass of bromine available in the magma reservoir prior to the eruptions under consideration. The discrepancy that we highlight between the mass of Br in the co-existing melt and fluid prior to the Merapi 2010 eruption (433 and 73 tons, respectively) and the lack of observed BrO (from space) hints at the need to investigate further Br speciation in 'ash-rich' volcanic plumes. Overall, our results suggest that the Br

50 yield into the atmosphere of cold and silicic magmas will be much larger than that from hotter
51 and more mafic magmas.

52

53 **Keywords:** bromine, fluid/melt partitioning, degassing, arc magmas, atmospheric chemistry

1. Introduction

Volcanic degassing is an important process in sustaining the composition of Earth's atmosphere (e.g., Gaillard and Scaillet, 2014; Mather, 2015). Whilst much progress has been made constraining global volcanic fluxes, uncertainties remain regarding the emissions of the key halogen species, especially the trace Br- and I-bearing species (Pyle and Mather, 2009). However, improvements in remote sensing techniques and analytical techniques, and their application to an increasing number of active volcanoes, have provided new data on the concentrations of these minor components in volcanic gases (e.g., Gerlach, 2004; Aiuppa et al., 2005; Aiuppa, 2009; Bobrowski et al., 2015), which in turn can be used to better constrain their global fluxes to the atmosphere (Pyle and Mather, 2009). Bromine has received particular attention over the last decade, owing to its important role in atmospheric chemistry in general (e.g., Oppenheimer et al., 2006; Roberts et al., 2009; 2014) and ozone depletion in the troposphere and stratosphere in particular (von Glasow et al., 2009; Kutterolf et al., 2013; Cadoux et al., 2015). Global compilations show that Br sources (emissions to the atmosphere) and sinks (removal routes from the atmosphere) are not strictly balanced, hinting at a missing natural source of Br (Montzka et al., 2011). The direct detection of HBr and BrO in volcanic plumes (Bobrowski et al., 2003; Aiuppa et al., 2005) suggests that volcanic activity may be one such a source.

The correct evaluation of the contribution of past volcanic eruptions to atmospheric chemistry depends on our ability to evaluate Br behaviour in magmas, in particular its partitioning between silicate melt and gas phases. So far, only a few experimental studies have been performed on this topic, and have investigated Br behaviour in synthetic albite to rhyolite melt compositions (Bureau et al., 2000; Bureau and Métrich, 2003). However, natural silicate melt compositions can depart significantly from such model systems, in particular by having elevated contents of Fe, Mg or Ca, which (as Na) can complex with halogens thereby

enhancing their solubility in silicate melts (Cochain et al., 2015). The relationship between halogen solubility and their complexation with cations has been shown for Cl; chlorine solubility in most silicate melts is dominantly controlled by the abundances of $Mg \sim Ca > Fe > Na > K > \text{network-forming Al} > Li \sim Rb \sim Cs$, but Ti, F, and P also have strong influences (e.g., Webster et al., 1999; Webster and De Vivo, 2002). There is thus a need to evaluate the role of melt composition on Br behaviour in magmas, which is the main motivation of the present study. To that end, we have performed fluid/melt partitioning experiments on natural basalt, andesite and rhyodacite compositions under P-T-H₂O-redox storage conditions relevant to shallow arc magmas. Combining our Br partition coefficient for the basaltic composition, with other experimental data on S and Cl behaviour, and volcanic gas compositions from the literature, we develop a simple first-order model to predict the S-Cl-Br degassing behaviour in mafic systems. We also measure Br contents of melt inclusions from Etna, Stromboli, Merapi and Santorini eruptions and estimate the mass of bromine in the pre-eruptive magmas, this allows us to address the atmospheric contribution of open-vent mafic volcanoes versus that of intermediate-silicic volcanoes.

2. Fluid/melt partitioning experiments

2.1 Starting material

The selected starting materials are natural volcanic rocks: a hawaiitic basalt from a 2002 Etna eruption (Lesne et al., 2011a, b; Iacono-Marziano et al., 2012), a calc-alkaline andesite and a rhyodacite from the Santorini Upper Scoria-2 (USC-2) and Minoan eruptions, respectively (Cadoux et al., 2017). The whole-rocks were crushed and ground in an agate mortar. About 10 g of the powders were melted twice (and ground in between), to ensure homogenization, in a platinum crucible at 1400 °C - 1 atm for 3-4 hours in a piezoceramic oven, and quenched in

cold water. The resulting dry glasses were ground to powder and constituted the starting material for both (i) bromine standard glasses synthesis (Cadoux et al., 2017) used to calibrate bromine analyses (section 3) and (ii) partitioning experiments. The compositions of the starting glasses are given in Table 1.

2.2 Experimental procedure

Equilibrium partitioning experiments (neglecting kinetic effects) were performed in an Internally Heated Pressure Vessel equipped with a rapid quench device at the Institut des Sciences de la Terre d'Orléans (ISTO, Orléans, France). The chosen experimental T-P- fO_2 conditions are representative of those in shallow crustal reservoirs in volcanic arc contexts (Martel et al., 1999; Di Carlo et al., 2006; Cadoux et al., 2014; Kahl et al., 2015) and are reported in Table 2: T ($\pm 10^\circ\text{C}$) = 900, 1060 and 1200°C , P ($\pm 2\text{ MPa}$) = 100 and 200 MPa, and fO_2 estimated around the Ni-NiO (NNO) buffer, on the basis of the partial pressure of H_2 imposed in the vessel (~ 2 bars; Di Carlo et al., 2006; Cadoux et al., 2014).

We deliberately used a fluid solely composed of H_2O and Br. Experiments with simplified fluids are necessary for comparison with future experiments which will include additional volatile species (e.g., CO_2 , S), and will permit us to assess whether or not the presence of other volatile species can modify Br behaviour.

Capsules were always loaded so that the mass ratio between the aqueous fluid and the glass (silicate) phases was equal to or lower than 0.1 (Table 2), which avoids significant silicate dissolution into fluid during experiments. About 50 to 100 mg of glass powder was loaded into Au or Au-Pd capsules (2.5 mm internal diameter, 20-30 mm in length) together with 3-8 mg of a solution composed of distilled water and dissolved NaBr salt. These amounts of solution (6-10 wt%) ensure the attainment of fluid saturation of the silicate melts at the investigated T-P conditions. Different solutions with Br contents between 0.1 and 14 wt% Br

were employed. The runs lasted between 24 and 92 hours, depending on the temperature (Table 2). Chlorine partitioning experiments of Alletti et al. (2009) performed at 1200°C with a basaltic melt showed that 3-4 hours were sufficient to attain equilibrium at 1200°C and $P > 1$ MPa. Considering that Br diffusion coefficient appears to be 2–5 times lower than the other halogens in basaltic melts (at 500 MPa to 1.0 GPa, 1250 to 1450 C and at anhydrous conditions, Alletti et al., 2007), we chose a 24 hour run duration for our experiments at 1200°C-100 MPa including the basaltic composition, to ensure the attainment of equilibrium. For our experiments at 900°C- 200 MPa including the silicic composition, a run duration of 92 hours was chosen on the basis of previous experiments with chlorine. Kravchuk and Keppler (1994) performed partitioning experiments with silicic melts at lower T (800°C) and same P with duration varying between 93h to 1142h, which yielded similar results, thus demonstrating that 93h was sufficient to attain equilibrium (at 800°C). The run duration for the experiment at 1060°C (48h) with andesite and rhyodacite compositions was chosen as intermediate between that at 900°C and that at 1200°C. Experiments were terminated by drop quench (Di Carlo et al., 2006). Upon opening the capsules, hissing and fluid escape occurred, indicating the presence of excess fluid, and thus that fluid saturation was achieved at the target P-T conditions. All runs produced crystal-free glasses, those of rhyodacitic composition being rich in fluid inclusions (Fig. A.1 in Supplementary Material).

3. Analytical techniques

3.1. Major element analysis

Experimental glasses and natural melt inclusions were analysed for their major elements by electron microprobe (EMP) using the joint ISTO-BRGM SX-Five microbeam facility

(Orléans, France). The operating conditions were: 15 kV accelerating voltage, 4-6 nA beam current, 10 seconds counting time on peaks, 5 seconds on background. The standards used were: albite for Si and Na, TiMnO_3 for Ti and Mn, Al_2O_3 for Al, Fe_2O_3 for Fe, MgO for Mg, andradite for Ca and orthose for K. Alkalis were analyzed first and a defocused beam was used to minimize alkali migration: 20 μm diameter for experimental glasses, and 6-10 μm for melt inclusions. Between 5 and 10 analyses were performed on each charge. The EMP detection limit for Na (component of the aqueous solution used in the experiments and thus considered in the calculation of the Br partition coefficients; Supplementary Information) was generally < 700 ppm.

3.2. Volatile analysis

Br abundances in the experimental glasses were determined either by Laser Ablation Inductively Coupled Plasma Mass Spectrometry (LA-ICP-MS) or with a Secondary Ion Mass Spectrometer (SIMS), using Br glass standards synthesized with the same starting compositions as those used for the partitioning experiments presented here (Table 1, Cadoux et al., 2017). LA-ICP-MS has been shown to be a technique suited to analyse Br contents of hundreds to thousands ppm in experimental glasses, while SIMS and synchrotron X-ray fluorescence (SR-XRF) are more appropriate techniques for lower Br contents (Cadoux et al., 2017). Moreover, the spatial resolutions of SIMS and SR-XRF are significantly higher than that of LA-ICP-MS (Cadoux et al., 2017), we therefore analysed bromine contents in melt inclusions from Santorini, Merapi and Etna volcanoes by SIMS and SR-XRF.

The abundance of water dissolved in most of the experimental glasses was determined by SIMS.

3.2.1. Bromine analysis by LA-ICP-MS

LA-ICP-MS analyses were performed at the Istituto Nazionale di Geofisica e Vulcanologia (INGV, Palermo, Italy). The laser used is a Compex Pro 102, 193 nm ArF excimer laser mounted on an ablation system GeoLas Pro, which is connected to an Agilent 7500ce ICP-MS. Analyses were done on polished glass chips set in epoxy resin.

Analyses were performed with a fluence of 15 J/cm² and a pulse energy of 100 mJ. The samples were ablated during ~50 seconds on a 90 µm diameter area, with a pulse repetition rate of 10 Hz. Three to ten analyses were collected for every sample, to check sample homogeneity. With this configuration, Br contents of >100 ppm are quantifiable with accuracy generally within 20% (Cadoux et al., 2017).

Data reduction was performed using GLITTER™ software (Griffin et al., 2008), using ²⁴Mg as the reference element (Mg contents from EMP analyses), and in-house bromine glass standards B3000 and B6000 (with 2694 ± 5.1 and 5968 ± 3.5 ppm Br, respectively; Cadoux et al., 2017), as external standards. The error on the measured ⁷⁹Br/²⁴Mg ratio was always < 4%.

3.2.2. Bromine analysis by SIMS

Polished chips of experimental glasses were set into indium and coated with gold, while individual crystals from Santorini Minoan eruption, Merapi 2010 eruption and Etna 2006 eruption were mounted in epoxy resin, polished and coated with gold for melt inclusion analysis.

Analyses were conducted at the Centre de Recherches Pétrographiques et Géochimiques (CRPG, Nancy, France) with a Cameca IMS 1280 HR2. The Cs⁺ primary ion beam was accelerated at 10 kV with an intensity of 5 nA, and focused on a 15 µm diameter area. The electron gun was simultaneously used for charge compensation. Negative secondary ions were extracted with a 10 kV potential, and the spectrometer slits set for a mass resolving power (MRP = M/ΔM) of ~20,000. A single collector (EM) was used in ion-counting mode,

and the spectrum scanned by peak jumping. Each analysis consisted of 8 or 6 successive cycles. Each cycle began with background measurement at the mass 75.8, followed by $^{28}\text{Si}^{16}\text{O}_3^-$ (75.963 amu), $^{30}\text{Si}^{16}\text{O}_3^-$ (77.959 amu), $^{79}\text{Br}^-$ and $^{81}\text{Br}^-$, with measurement times of 4, 4, 4, 10 and 30 s, respectively (waiting time of 2 s). More details about the analytical configuration can be found in Cadoux et al. (2017).

We used three different sets of in-house bromine glass standards (Cadoux et al., 2017): a basaltic set containing 1 to 6,000 ppm Br (B1 to B6000), an andesitic set containing 10 to 1,000 ppm Br (A10 to A1000), and a rhyodacitic set containing 10 to 5,000 ppm Br (RD10 to RD5000).

The bromine content of the samples was calculated using the measured $^{81}\text{Br}/^{28}\text{SiO}_3$ and known Br (ppm)/ SiO_2 (wt%) ratios of the standards (Cadoux et al., 2017).

The three glass sets define distinct linear calibration curves with slopes decreasing with increasing degree of melt polymerization (Cadoux et al., 2017). The equation of the calibration lines passing through zero is:

$$\left(\frac{^{81}\text{Br}}{^{28}\text{SiO}_3}\right) = a \left(\frac{\text{Br}}{\text{SiO}_2}\right)$$

where the slope a is a function of SiO_2 content.

The error on the measured $^{81}\text{Br}/^{28}\text{SiO}_3$ ratio was generally $< 3\%$ (most often $< 2\%$).

3.2.3. Br analysis by SR-XRF

Bromine in Etna and Stromboli melt inclusions was analysed via SR-XRF at the UK national synchrotron facility, Diamond Light Source (Didcot, Oxfordshire), on I18, the Microfocus Spectroscopy beamline. Analyses were performed on polished olivine-hosted melt inclusions set in epoxy resin, using a beam of $\sim 5 \times 5 \mu\text{m}^2$ and an analysis time of 120 s (details in Cadoux et al., 2017). Fluorescence spectra were processed by PyMca (Solé et al.,

2007), by identifying the K-lines of Br and applying an iterative Gaussian peak fitting procedure to quantify the net peak areas free of background and interference from other elements.

Background- and baseline-subtracted net peak areas for the MI samples were converted into Br concentrations from comparison with peak areas measured for the basaltic standards of known Br composition (Cadoux et al., 2017). Based on tests made on the standards (Cadoux et al., 2017), the Br detection limit is inferred to be < 1 ppm, Br contents ≤ 5 ppm (representative of Br contents in most natural volcanic glasses) are measured with an accuracy $< 26\%$ and with a precision of 30%.

3.2.4. Water analysis by SIMS

The analysis of water dissolved in the experimental glasses was performed on the CRPG Cameca 1280 HR2. Spot analyses of secondary ions ^{17}O , $^{16}\text{O}^1\text{H}$, ^{18}O , ^{29}Si , ^{30}Si were obtained using a 3 nA, 20 μm diameter primary beam of Cs^+ ions. The electron gun was simultaneously used for charge compensation. The measurements were made at a mass resolution of $\sim 7,700$ to separate $^{17}\text{O}^-$ and $^{16}\text{O}^1\text{H}^-$. An energy filtering was set at $+30 \pm 10$ eV in moving the energy slit off axis, to minimize both matrix effect and instrumental background. A 10×10 μm raster was used for 1 minute prior to analysis at each spot in order to pre-sputter through the gold coat and remove surface contamination. The beam position in the field aperture and the magnetic field centering was checked before each measurement. Each analysis on one spot consisted of 18 cycles of measurements, with counting times and switching times of 3 and 1 s respectively at each peak. The errors on the measured $^{16}\text{O}^1\text{H}/^{30}\text{Si}$ ratios were $< 1\%$.

Concentrations of H_2O were calculated using a best-fit quadratic polynomial regression to count-rate ratios (normalized to ^{30}Si) versus variable known concentration ratios (referenced

to wt% SiO₂) of experimental glass standards of basaltic (sample N72, Kamtchatka; Shishkina et al., 2010), trachy-andesitic (sample TAN25, Tanna Island, Vanuatu; Metrich & Deloule, 2014), dacitic and rhyolitic (Pinatubo, Philippines; Scaillet & Evans, 1999) compositions, with H₂O contents ranging from 0 to ~6 wt%.

4. Results

4.1. Major element compositions

Average major element compositions of experimental glasses and melt inclusions are presented in Tables 3 and A2, respectively. Comparison of the experimental products (Table 3) with the corresponding starting dry glasses (Table 1) shows a systematic gain in Na₂O due to the addition of sodium through the H₂O-NaBr solution in the experimental charges (10 to 153 µg of Na were incorporated into the final glass, Table A.1), and a loss in FeO (up to 14% taking into account standard deviations) in experiments ≥ 1060 °C, most likely due to Fe alloying with the AuPd capsule. Other elements were generally comparable with the starting glasses within standard deviations.

4.2. H₂O and Br dissolved in experimental glasses

The concentrations of both H₂O and Br dissolved in quenched glasses are reported in Table 2. Melt water contents (H₂O_{melt}) vary between 2.9 up to 7.3 wt%, encompassing the range of pre-eruptive H₂O_{melt} of arc magmas (e.g., Scaillet et al., 1998; Di Carlo et al., 2006; Cadoux et al., 2014). Bromine concentrations range from 69 (M4-RD1; Table 2) to 9112 ppm (M2-B), comparable to the range explored in previous experimental studies (Bureau et al., 2000; Bureau and Métrich, 2003). Repeat analyses of either H₂O (n = 5-7) or Br (n = 3-10) in quenched glasses show them to be homogeneous within analytical uncertainty (including error on calibration and error on sample measurements), indicating that the run durations (1 to 4

days according to T-P conditions; Table 2) were sufficient to attain chemical equilibrium between the co-existing melt and fluid phases.

4.3. *Fluid/melt bromine partitioning*

Assessment of the partition coefficients requires the calculation of the ratio between Br concentration (in ppm) in coexisting aqueous fluid and silicate melt at the experimental conditions. In natural magmatic systems, besides from being dissolved in the silicate melt, Br can exist as a gas species in the vapour phase and/or be dissolved in hydrosaline liquid phase (brine), as has been shown for Cl. This raises the question as to whether a brine rich in Br could have been present in our capsules at run conditions. Solubility experiments of Bureau et al. (2003) have shown that silicic melts can contain up to 7850 ppm Br at P-T conditions of 100-200 MPa and 900-1080°C without brine occurrence. Our experiments were run at similar conditions, with Br contents lower than 2000 ppm (Table 2). We thus conclude that our silicic melts did not co-exist with a brine, and that only a gas phase was present. There is no data about Br solubility in mafic melts but the results of our experiment #3 (basalt, andesite, rhyodacite in the same experimental P-T-H₂O-[Br^o] conditions; Table 2) suggest a higher ability for Br to enter in mafic melts, so that, by comparison with the values for silicic melts given above, we might expect that brine saturation in andesitic and basaltic melts occurs for Br contents higher than 8000 ppm. Hence, as for the silicic melts, we conclude that basaltic-andesitic charges were co-existing solely with a gas phase during the experiments.

Whereas the amount of Br dissolved in the melt ([Br]_{melt}) was directly analysed (by SIMS or LA-ICP-MS in run product glasses, section 3; referred to as '[Br] measured in final glass' in Table 2), the Br amount of the coexisting aqueous fluid phase ([Br]_{fluid}) was determined by mass balance, knowing the original bulk Br content (the amount of Br loaded in the capsule as H₂O+NaBr solution; hereafter [Br^o]), the measured amount of Br dissolved in the final glass

302 ([Br]_{melt}), and assuming that the difference between these two figures represents the amount of
 303 Br left over for the fluid phase.(details of the calculation are given in Supplementary
 304 Information and in Table A.1). For each run product, we estimated the errors on the calculated
 305 [Br]_{fluid} and $D_{Br}^{f/m}$ by propagating the errors coming from the preparation of the experimental
 306 charges to the analysis of Br, Na and H₂O contents of the glasses (Supplementary Information
 307 and Table A.1). The resulting errors on [Br]_{fluid} are < 51% (and mostly < 34%), except for one
 308 run-product (M1-B). As the main source of error for $D_{Br}^{f/m}$ is [Br]_{fluid}, the resulting errors on
 309 $D_{Br}^{f/m}$ are close to those for [Br]_{fluid}: they do not exceed 54% and are mostly <45%, except for
 310 M1-B (112%; Table A.1). Note that, as underlined in previous studies (e.g., Alletti et al.,
 311 2014), such rigorous error propagation overestimates the real errors, due to the complex
 312 covariation of individual errors. The large error associated with the $D_{Br}^{f/m}$ estimated for M1-B
 313 is due to the low fluid/melt mass ratio of the experimental charge (0.06 compared to 0.08-0.11
 314 for the others): the mass of initial fluid is small relative to the weighing error (Table A1).
 315 Therefore, the calculated mass of fluid has a larger associated relative error of 19% (<15% for
 316 the other run products), which increases the error on the calculated value for [Br]_{fluid} and
 317 $D_{Br}^{f/m}$. This observation is consistent with the uncertainty analysis for the mass balance
 318 calculations of Zajacz et al. (2012), which shows that the determination of D for elements
 319 with low D values in experiments with low volatile/mass ratio may bear large uncertainties
 320 due to error propagation. Their modeling (Fig. 1 in Zajacz et al., 2012) predicts relative error
 321 of 10 up to 100% for volatile/mass ratios lower than 0.1. The error on the $D_{Br}^{f/m}$ estimated for
 322 M1-B being > 100% ($D_{Br}^{f/m} = 3.8 \pm 4.5$), we conclude that this value, taken alone, is
 323 meaningless. Overall, the error on $D_{Br}^{f/m}$ is particularly sensitive to the error on the measured
 324 [Br]_{melt} (i.e., Br content of the run product glasses). The precision of the Br measurements is
 325 crucial for the accuracy of $D_{Br}^{f/m}$.

326 The main data of the partitioning experiments are listed in Table 2 (details in Table A1) and
 327 displayed on Figures 1 to 5.

328 The basaltic products of runs #1 to 3 performed at 1200°C, 100 MPa, with various $[\text{Br}^\circ]$
 329 contents apparently show a linear relationship between the measured $[\text{Br}]_{\text{melt}}$ and the
 330 calculated $[\text{Br}]_{\text{fluid}}$ (Fig. 1). Linear regression forced through zero yields a $D_{\text{Br}}^{f/m} = 5.0 \pm 0.3$
 331 for the basaltic composition. At the same T-P- $[\text{Br}^\circ]$ conditions (experiment #3; Table 2),
 332 $D_{\text{Br}}^{f/m}$ increases steadily from basalt ($D_{\text{Br}}^{f/m} = 4.6 \pm 2.0$), to andesite ($D_{\text{Br}}^{f/m} = 6.4 \pm 3.5$), to
 333 rhyodacite ($D_{\text{Br}}^{f/m} = 11.3 \pm 0.9$). At 1060°C, 200 MPa, ~NNO (Fig. 2), experiments on
 334 andesite and rhyodacite melts yields linear trends between $[\text{Br}]_{\text{melt}}$ and $[\text{Br}^\circ]$ (Fig. 2a) or
 335 $[\text{Br}]_{\text{fluid}}$ (Figs. 2b and 2c). Linear regression of the latter data forced through zero yields $D_{\text{Br}}^{f/m}$
 336 $= 9.1 \pm 0.6$ for andesite, and $D_{\text{Br}}^{f/m} = 14.0 \pm 0.6$ for rhyodacite. At 900°C - 200 MPa, (Fig. 3),
 337 the same pattern is again observed resulting in $D_{\text{Br}}^{f/m} = 20.2 \pm 1.2$ for rhyodacite, slightly
 338 higher than that of Bureau et al. (2000) for albitic melts (17.5 ± 0.6).

339 The experiments show a two-fold increase of $D_{\text{Br}}^{f/m}$ from basalt (5.0 ± 0.3) to rhyolite melts
 340 (11.3 ± 0.9) at 1200°C - 100 MPa (Fig. 4). The same trend of an increase of $D_{\text{Br}}^{f/m}$ with SiO_2
 341 is noted at 1060°C - 200 MPa, with a slightly higher slope. At 900°C, we did not work on
 342 basaltic/andesitic compositions because of their extensive crystallization (which would have
 343 driven the residual liquids toward higher SiO_2 content). Our data on silicic compositions,
 344 along with those of Bureau et al. (2000) (Fig. 4), suggest a similar trend of increasing $D_{\text{Br}}^{f/m}$
 345 with increasing SiO_2 at 900°C. Figure 4 also suggests a general trend of an increase in $D_{\text{Br}}^{f/m}$
 346 as temperature decreases, at least for more silicic compositions. For instance, for rhyolitic
 347 melts (71 wt% SiO_2), a linear extrapolation of our data set ($D_{\text{Br}}^{f/m} = -0.0299 \times T(^{\circ}\text{C}) + 46.673$,
 348 $r^2 = 0.97$) yields $D_{\text{Br}}^{f/m} = 26$ at 700°C (Fig. 5).

349 We did not attempt to explore the effect of pressure in a systematic way. Previous work has
 350 shown that $D_{\text{Br}}^{f/m}$ strongly increases as pressure decreases, from about 20 at 200 MPa up to

over 300 at near atmospheric pressure in silicic melts (synthetic haplogranitic composition; Bureau et al., 2010). In contrast, our experiment at 100 MPa (experiment #3) does not show any significant increase in $D_{\text{Br}}^{f/m}$, with $D_{\text{Br}}^{f/m}$ being instead generally lower than those at 200 MPa (experiments #4 and #5; Table 2). However, the fact that temperatures between our 100 and 200 MPa runs are different, does not allow us to make definitive conclusions on this aspect. We suggest that our results should be used to model degassing processes in the crustal reservoir and not for simulating decompression processes between the reservoir and surface.

4.4. *Br contents in melt inclusions*

Table A.2 reports the Br contents of melt inclusions from (i) basaltic magmas erupted at Mount Etna and Stromboli, (ii) the andesitic magma erupted in 2010 at Mount Merapi, and (iii) the rhyodacitic magma of the 1613 BC Minoan eruption of Santorini volcano. Melt inclusions from Mt. Etna and Stromboli are hosted by olivine crystals, while those from Mt. Merapi and Santorini volcano are in pyroxenes and plagioclase crystals, respectively. Br abundance ranges from 2.5 to 10 ppm, without any clear correlation with melt inclusion major element composition; there is no notable difference between basaltic, andesitic and rhyodacitic melt inclusions. The Br contents of these melt inclusions are comparable to those of submarine back-arc and arc glasses (Kendrick et al., 2014).

5. Discussion and applications

5.1. *Halogen behaviour*

This section aims to place our novel Br partitioning data in the wider framework of halogen behaviour. Hereafter, we provide a brief, non-exhaustive review of chlorine, fluorine and iodine partitioning and make comparisons with bromine.

Many studies have been dedicated to understanding the partitioning behaviour of halogens between fluids and silicate melts (e.g., Webster, 1990; Webster and Holloway 1990; Webster 1992a,b; Webster et al. 1999; Signorelli and Carroll, 2000; Bureau et al., 2000; Botcharnikov et al., 2004, 2007, 2015; Dolejs and Baker 2007a,b; Alletti, 2008; Stelling et al. 2008; Chevychelov et al., 2008b; Webster et al., 2009; Borodulin et al., 2009; Alletti et al. 2009, 2014; Beermann 2010; Zajacz et al. 2012; Webster et al., 2014; Beermann et al., 2015). Nevertheless, most of these studies have focused on chlorine, mainly because of its importance as a ligand for ore metals (e.g., Carroll and Webster, 1994; Aiuppa et al., 2009).

5.1.1 General behaviour

Chlorine partitions preferentially into fluids relative to melts for the vast majority of terrestrial magmas at shallow-crustal pressure and temperature conditions, due to its highly solubility in aqueous and aqueous-carbonic fluids (e.g., Webster et al., 2018 and references therein). The few partitioning experiments performed with bromine and iodine show a similar behaviour (Bureau et al., 2000; Bureau et al., 2016; this study). In contrast, fluorine concentrations in aqueous and aqueous-carbonic fluids at magmatic conditions are much lower than those of the other halogens (e.g., Carroll and Webster, 1994), and can be therefore enriched in the silicate melt with respect to the fluid phase (e.g., Webster, 1990; Webster and Holloway 1990).

5.1.2 The effect of melt composition

In this study, we show that the partitioning of bromine between aqueous fluid and melt appears to be influenced by the melt composition (Figs. 1, 2, 4). We estimate $D_{\text{Br}}^{f/m}$ of 4.6 ± 2.0 , 6.4 ± 3.5 and 11.3 ± 0.9 for basaltic, andesitic and rhyodacitic compositions respectively, with $[\text{Br}^\circ] = 2.4 \text{ wt.}\%$, at 1200°C , 100 MPa and $f\text{O}_2$ close to NNO (exp. #3, Table 2). If $D_{\text{Br}}^{f/m}$ of the basalt and andesite are comparable taking into account the error bars, the difference

401 between the mafic-intermediate compositions on one hand, and the silicic composition on the
 402 other hand, is significant. In addition, we observe the same trend at 1060°C, 200 MPa where
 403 $D_{\text{Br}}^{f/m}$ of the silicic composition (14.0 ± 0.6) is significantly higher than that of the
 404 intermediate composition (9.1 ± 0.6). This relationship between melt composition and Br
 405 partitioning is consistent with the higher Br solubility in melts with lower SiO_2 observed by
 406 Bureau and Métrich (2003). The recent study of Cochain et al. (2015) on Br speciation in
 407 hydrous alkali silicic melts at high pressure (up to 7.6 GPa) confirms this trend. Similarly,
 408 several studies have demonstrated the strong effect of melt composition on fluid/melt
 409 partitioning of chlorine (Webster 1992a,b; Webster et al. 1999). Like $D_{\text{Br}}^{f/m}$, $D_{\text{Cl}}^{f/m}$ also
 410 increases with increasing SiO_2 contents of the melts (i.e., with increasing melt polymerization
 411 and thus decreasing Br and Cl solubility in melt; e.g., Webster, 1992a,b; Signorelli and
 412 Carroll, 2000; Botcharnikov et al., 2004; Webster, 2004; Webster et al., 2006; Webster et al.,
 413 2009). Most experimental values of $D_{\text{Cl}}^{f/m}$ for basaltic systems are <10 (Stelling et al 2008;
 414 Beermann 2010; Baker and Alletti 2012), but Alletti et al. (2009) observed $D_{\text{Cl}}^{f/m}$ of 8-34 in
 415 trachybasaltic melt in equilibrium with aqueous fluids at $f\text{O}_2$ near NNO. Values of $D_{\text{Cl}}^{f/m}$ for
 416 intermediate (andesitic and phonolitic) and silicic melts exceed those for mafic melts (e.g.,
 417 Webster et al. 1999; Stelling et al., 2008; Chevychelov et al., 2008b; Alletti et al., 2009;
 418 Beermann, 2010; Beermann et al., 2015); with values >160 determined for silicic melts at 200
 419 MPa (Webster, 1992a). Note that $D_{\text{Cl}}^{f/m}$ also varies strongly with Cl concentration (Webster
 420 1992a,b; Webster et al. 1999; Stelling et al. 2008) and a decrease of $D_{\text{Cl}}^{f/m}$ by up to the order
 421 of one magnitude can be observed when the Cl concentration in the system decreases (from
 422 several wt.% to <1 wt.% Cl). At low Cl system concentrations (<1 wt% Cl in andesite, Zajacz
 423 et al., 2012; or in basalt, Beermann et al., 2015; Stelling et al., 2008), $D_{\text{Cl}}^{f/m}$ seems to achieve
 424 values close to or even below unity. From our data, we do not observe any systematic
 425 relationship between Br concentration in the system ($[\text{Br}^\circ]$) and $D_{\text{Br}}^{f/m}$: the apparent decrease

of D-values for andesite (M4-A) relative to $[Br^o]$ at 1060°C and 200 MPa (Table 2) is actually not significant taking into account the errors on D. More experiments are necessary to investigate the potential relationship between $D_{Br}^{f/m}$ and the Br concentration in the system. Unlike bromine and chlorine, values of $D^{f/m}$ for fluorine are lower in silicic melts (typically well below unity; Webster, 1990; Webster and Holloway 1990; Dolejs and Baker 2007a,b; Borodulin et al., 2009) than in mafic melts coexisting with aqueous fluids (ca. 3 to 38; Alletti, 2008; Chevychelov et al., 2008b).

5.1.3 Temperature and pressure effects

Our data suggest that $D_{Br}^{f/m}$ is sensitive to melt temperature (increase of $D_{Br}^{f/m}$ with decreasing temperature; Figs. 4 and 5), though more experiments are required to confirm this trend. Currently there are insufficient data available to constrain the temperature effect for the other halogens. The few existing data concern Cl in phonolitic and trachybasaltic melts and suggest that there is no strong influence of temperature (Chevychelov et al., 2008a; Stelling et al., 2008).

We do not systematically investigate the effect of pressure on $D_{Br}^{f/m}$. Experiments conducted on haplogranite melts coexisting with iodine-bearing aqueous fluids indicate an increase of $D^{f/m}$ of iodine with pressure decrease (from ~2 at 1.5 GPa to 41 at 0.1 GPa; Bureau et al., 2016). Contrastingly, $D^{f/m}$ of fluorine decreases with decreasing pressure as suggested by experiments on trachybasaltic melts (Alletti, 2008; Chevychelov et al., 2008b). Available data for chlorine show no clear pressure effect on $D_{Cl}^{f/m}$ for most compositions and contrasting effects for phonolitic ones (Signorelli and Carroll, 2000; Baker and Alletti, 2012; Alletti et al. 2014).

We conclude that more systematic experiments are necessary for all halogens to assess the effect of pressure and temperature on their fluid/melt partitioning, in order to interpret degassing processes of ascending and cooling magmas comprehensively.

5.1.4 Effect of fluid composition

Experiments with trachybasaltic melts coexisting with aqueous fluids have shown that the addition of CO₂ to the system leads significant reductions of $D^{f/m}$ of fluorine.

Several studies have investigated the effect of fluid composition on Cl partitioning in chemically complex O-H ± C ± S ± Cl fluids and show variable influence of CO₂ or S on $D_{Cl}^{f/m}$, no systematic trend appears (e.g., Botcharnikov et al. 2004; Webster et al. 2003; Botcharnikov et al., 2007; Alletti et al., 2009; Beermann 2010, Zajacz et al. 2012; Webster et al., 2014). As we do not explore the effect of other volatile species on Br partitioning in this study, we will not enter into the details of those studies (for a review on this topic, see Webster et al., 2018). Clearly, further investigations are needed to better understand the effects of other volatile species on halogens partitioning.

5.1.5 Role of ionic radius?

On the basis of their results ($D_{Cl}^{f/m} = 8.1$, $D_{Br}^{f/m} = 17.5$, $D_I^{f/m} = 104$ with an albitic melt), Bureau et al. (2000) suggested that bromine and iodine partitioned even more strongly into the fluid phase than chlorine and that it could be correlated to the increasing ionic radius of the halide ions ($Cl^- = 1.81 \text{ \AA}$, $Br^- = 1.96 \text{ \AA}$, $I^- = 2.20 \text{ \AA}$; Shannon, 1976). Nevertheless, our brief review above shows that chlorine fluid/melt partition coefficients as high as that of iodine may be reached with a rhyodacitic melt ($D_{Cl}^{f/m} = 115$, Table 2 in Webster et al., 2009) depending on the initial Cl content in the bulk system. In addition, we show in section 5.2. below that the range of Br and Cl composition of volcanic gases and melts from mafic

systems requires a lower $D_{\text{Br}}^{f/m}$ ($= 5$) than the $D_{\text{Cl}}^{f/m}$ value (8.6); this questions the general applicability of the higher volatility of Br as shown by the experimental results of Bureau et al. (2000) and Mungall and Brenan (2003) and attributed to the larger ionic radius of Br vs. Cl.

5.2. *S-Cl-Br degassing behaviour in mafic magma systems*

Our partition coefficients for Etnean melts set the basis for initializing the first basic models to evaluate Br degassing behaviour in mafic systems. Our aim is to derive model-based evidence for Br abundance in magmatic gases coexisting with mafic melts at shallow crustal conditions, and to compare this with available information on the measured compositions of volcanic gases, the ultimate product of magmatic degassing. Figure 6a shows a selection of volcanic gas plume compositions (in the S-Cl-Br system) from some open-vent mafic volcanoes (for data provenance, see caption of Figure 6). The wide range of volcanic gas S/Br compositions observed points to a mechanism fractionating Br, relative to sulfur, during magmatic degassing or systematic variations in melt compositions, e.g., between different tectonic settings. In comparison, volcanic gases exhibit a far more restricted range of Cl/Br ratios (see Fig. 6a and Gerlach, 2004; Aiuppa et al, 2005, 2009; Webster et al., 2018), which suggests that less Cl/Br fractionation takes place during degassing and/or less comparative variation in melt compositions. The relatively constant Cl/Br ratios in our gas dataset also indicate that Cl vs. Br decoupling due to fractionations among coexisting brine and vapour (Foustoukos and Seyfried, 2007; Seo and Zajacz, 2016), or by halite precipitation (Foustoukos and Seyfried, 2007), are unlikely to occur at the mafic, halogen-poor melt conditions explored here (Webster et al., 2009, 2018). We consider below our new Br partitioning data, in tandem with previous information on S and Cl from the literature, to provide a simple model verification for these volcanic gas-based inferences.

Rigorous quantitative calculation of magmatic gas compositions would require a theoretical and/or empirical model that describes solubilities, fluid/melt partition coefficient, and diffusivities of all involved volatiles over the range of P-T-X conditions experienced by magmas upon ascent, storage, and eruption. Such quantitative information is increasingly available for S (see review of Baker and Moretti, 2011), still limited for Cl (Webster et al., 1999, 2015, 2018), but virtually absent for Br. Given this limitation, we base our model calculations on a modified version of the empirical degassing model of Aiuppa et al. (2002) and Aiuppa (2009). The original model described the evolution of the SO₂-HCl-HF magmatic gas phase exsolved during progressive degassing of a basaltic magma, using a Rayleigh-type open-system degassing model assumption, and with constant S, Cl and F fluid/melt partition coefficients. Based on fair agreement between model results and volcanic gas compositions, it was concluded that a Rayleigh-type open-system process could suitably reproduce the relatively shallow exsolution of halogens from basaltic magmas that often dominates the gas signature (Métrich and Wallace, 2008; Métrich et al., 2001, 2004, 2010; Spilliaert et al., 2006; Edmonds et al., 2009; Webster et al., 1999, 2015; Mather et al., 2012).

Here we adapt and extend the methodology of Aiuppa (2009) to bromine, and develop a simple model to account for the variability of S-Cl-Br compositions of volcanic gases (Fig. 6a). We use similar sets of Rayleigh-type open-system equations as in Aiuppa (2009) but, contrarily to previous work, we do not derive fluid/melt partition coefficients using an empirical best-fit procedure to volcanic gas data, but rather use independent information (from Alletti et al., 2009; Aiuppa, 2009; and this work) (see below).

We use equations (1) and (2) to calculate the evolving S/Cl and S/Br (molar) ratios in the magmatic gas phase produced upon increasing extents of degassing of a mafic silicate melt:

$$\left(\frac{S}{Cl}\right)_{\text{gas}} = \left(\frac{S}{Cl}\right)_{\text{melt}_0} \cdot \frac{D_S}{D_{Cl}} \cdot R^{\left(1 - \frac{D_{Cl}}{D_S}\right)} \quad (1)$$

$$\left(\frac{S}{Br}\right)_{\text{gas}} = \left(\frac{S}{Br}\right)_{\text{melt}_0} \cdot \frac{D_S}{D_{Br}} \cdot R^{\left(1 - \frac{D_{Br}}{D_S}\right)} \quad (2)$$

where $\left(\frac{S}{Cl}\right)_{\text{gas}}$ and $\left(\frac{S}{Br}\right)_{\text{gas}}$ are the molar volatile ratios in the gas phase; $\left(\frac{S}{Cl}\right)_{\text{melt}_0}$ and $\left(\frac{S}{Br}\right)_{\text{melt}_0}$ are the original volatile ratios in the parental (un-degassed) melt; D_S , D_{Cl} and D_{Br} are the fluid/melt (molar) partition coefficients for the three volatiles; and R is the residual fraction of sulfur in the melt (ranging from 1 at onset of degassing to 0 if S is totally exsolved from the melt).

To resolve the model equations, $\left(\frac{S}{Cl}\right)_{\text{melt}_0}$ and $\left(\frac{S}{Br}\right)_{\text{melt}_0}$ are here set at 1.7 and 1320, respectively, from the characteristic S (0.27 wt%), Cl (0.18 wt%) and Br (5.1 ppm) contents in our most primitive, un-degassed glass inclusions from Etna (inclusion E2 from the 2001 eruption; Table A.2). The molar fluid/melt partition coefficients are obtained from our experimental results on Etnean melts for Br ($D_{Br}^{f/m} = 5.0$ on weight basis; Fig. 1) and those of Alletti et al. (2009) for Cl ($D_{Cl}^{f/m} = 8.6$ on weight basis), obtained at the same pressure (100 MPa), temperature (1200°C), redox conditions (NNO) and melt composition. These conditions are appropriate to describe halogen behaviour in mafic magmas at shallow crustal conditions and to extrapolate to shallow degassing, in view of the minor pressure-dependence of halogen fluid/melt partition coefficients (Alletti et al., 2009). It is noteworthy that the experiments of Alletti et al., (2009) were run at the low Cl concentrations (< 0.4 wt %) typical of mafic (basaltic to andesitic) melts (Webster et al., 2009), similar to those characteristic of the volcanoes we report gas data for in Figure 6. At such Cl-under-saturated conditions (absence of brine formation) the minor (if any) dependence of $D_{Cl}^{f/m}$ on total Cl contents justifies the use of a constant $D_{Cl}^{f/m} = 8.6$ throughout the entire degassing path. For S, a fluid/melt partition coefficient of 86 (on weight basis) is adopted based on the results of

Aiuppa (2009), who found that volcanic gas measurements from Etna and several mafic arc volcanoes worldwide can satisfactorily be reproduced with a D_S/D_{Cl} ratio (ratio between fluid/melt weight partition coefficients) of 10. Our inferred $D_S = 86$ agrees well with results obtained from S thermodynamic modelling (Moretti and Ottonello, 2005) of Etna-like melts at $P \leq 100$ MPa, \sim NNO and ~ 3 wt.% H_2O (Aiuppa et al., 2007), and is within the range of D_S values (3-236, by weight) obtained by Beermann et al., (2015) in their partitioning experiments between fluid and Etna-like melts at 100-200 MPa, and at either reducing or oxidizing redox conditions. We are aware that, at redox conditions close to the sulfide-sulfate transition, such as at \sim NNO (Jugo et al., 2010), D_S can exhibit large variations for even subtle redox variations (Beermann et al., 2015), and that therefore keeping D_S constant in our model is an over-simplification that does not completely reflect the real S degassing behaviour in natural (basaltic) systems. However, incorporation of such complexities (including the non-linear S partition behaviour, and its dependence on the total S content in the system; Beermann et al., 2015) into an S-Cl-Br degassing model is currently hampered by our very preliminary understanding of Br partitioning behaviour. In view of this, we find it safer to assume a constant D_S value (of 86) in our preliminary model, keeping in mind that our inferred D_S/D_{Cl} ratio is derived from empirical fitting of hundreds of volcanic gas data, and is thus likely to describe the “averaged” S degassing behaviour in mafic systems at shallow ($<< 3$ km; Spilliaert et al., 2006) conditions relevant to halogen degassing.

With these numbers, and with R varied from 1 (start of degassing) to 0 (complete S exsolution from the melt), the magmatic *vapour model line* shown in Figure 6a is obtained. The evolving volatile composition of the coexisting melt is obtained by mass balance (e.g., by subtracting from the initial volatile contents, at each degassing step, the volatile fractions partitioned into the vapour phase), and is illustrated by the *melt model line* (solid red line) in Fig. 6b.

Our model results predict that the coexisting magmatic gas and melt (Fig. 6a, b) should both evolve with increasing degassing, from S-rich (*early gas* and *early melt*) to Cl-Br rich (relative to S) (*late gas* and *late melt*). The *vapour model line* reproduces the observed compositional range of volcanic gas samples from Etna and other mafic systems well (Fig. 6a). Our calculations, therefore, provide a first, though simplistic, model to interpret Br abundance in volcanic gases from basaltic systems. We propose that high S/Br (along with S/Cl ratios; Aiuppa, 2009) gas compositions reflect shallow degassing of fertile (volatile-rich) magmas in basaltic volcano plumbing systems; while more soluble Cl and Br will prevail in gas released by later degassing stages (e.g., during near-surface syn-eruptive degassing). Our conclusions are opposite to those of Bobrowski and Giuffrida (2012) who, based on observational evidence and use of BrO gas measurements (that under-estimate total Br), proposed that low S/Br ratios mark “deep” degassing episodes of fresh basaltic magmas (at Etna). We stress, instead, that our model calculations more closely reproduce the similar *shallow* degassing behaviour of Cl and Br, which is supported by the limited variability of Cl/Br volcanic gas ratios (Fig 6a). We caution, however, that additional experimental observations, especially at low pressure, and rigorous thermodynamic models, are required to more fully constrain the fate of Br during ascent and degassing of mafic melts.

Our *melt model line* also suitably reproduces the compositional trends exhibited by Etna’s and Stromboli’s melt inclusions (data from Table A.2). Curiously, a set of model calculations initialised as above but with initial volatile contents from Stromboli’s most primitive inclusion (ST82c 137; S = 0.2 wt.%; Cl = 0.17 wt.%; and Br = 4.8 ppm; Table A.2) output a *melt model line* (orange line) that is very close to the Etna-like model trend above (Fig. 6b). An additional set of two model lines, calculated using slightly different initial Br contents to encompass the whole range of glass inclusion compositions observed, are also illustrated in the Figure 6b (dashed lines).

5.3. Bromine contribution of volcanism to the atmosphere

Global compilations show that Br sources and sinks are not strictly balanced, hinting at a missing natural source of Br (Khalil et al., 1993; Montzka et al., 2011). Methyl bromide CH_3Br (mainly produced by marine phytoplankton, biomass burning and fumigants in agriculture) is the largest source of bromine to the atmosphere, and is believed to play a key role in tropospheric and stratospheric ozone depletion (e.g., Mano and Andreae, 1994; Warwick et al., 2006). However, methyl bromide alone cannot explain the total amount of active Br species involved in the ozone destruction process (e.g., Warwick et al., 2006). Following the first detection of bromine monoxide (BrO) in a volcanic plume (Bobrowski et al., 2003), volcanic degassing (both passive and active) has been recognized as a potentially major source of reactive bromine species to the atmosphere (e.g., Gerlach, 2004; Oppenheimer et al., 2006). Possible approaches to quantify the volcanogenic bromine contribution to the atmosphere include: (i) direct measurements from volcanic fumaroles and plumes or (ii) calculation from bromine contents of pre-eruptive melts (i.e., undegassed crystal-hosted melt inclusions). Below we apply the second approach to Etna, Merapi and Santorini volcanoes, and compare to direct gas measurements when possible.

5.3.1 Bromine emission from an open-vent mafic volcano: the case of Mount Etna

Mount Etna is a persistently degassing basaltic volcano with frequent eruptive activity. We measured the Br contents of olivine-hosted melt inclusions from the trachybasaltic magma erupted during the 2006 Etna eruptions (Table A.2). This eruptive period began in mid-July 2006 and continued intermittently for 5 months (Neri et al. 2006; Behncke et al., 2008); it was characterized by strombolian and effusive activity along fissures and at different vent

locations and by a short episode of lava fountaining (more details in Behncke et al., 2009 and references therein).

Br in the pre-eruptive magma versus Br released in the atmosphere

Taking into account (i) an average Br content of 5.6 ppm dissolved in the pre-eruptive melt (Table A.2), (ii) a ‘dense-rock equivalent’ (DRE) erupted volume of 0.012-0.013 km³ (Supplementary Information) and (iii) 25 vol% of phenocrysts (Ferlito et al., 2010), we estimate that 125-141 tons of Br were dissolved in the melt prior to the eruption (SI).

The bromine output (as BrO) of this eruptive period, calculated from gas monitoring data (using an average SO₂ flux of 3444 tons/day, from Aiuppa et al., 2008; and a molar volcanic gas BrO/SO₂ ratio of 1.1×10^{-4} ; from Bobrowski and Giuffrida, 2012) was 85 tons. However, this is a minimum estimate since BrO is not emitted directly from the magma, but forms by conversion from HBr after emission (e.g. Oppenheimer et al 2006; Martin et al., 2009; von Glasow, 2010; Roberts et al., 2014). Thermodynamic equilibrium calculations indicate that HBr is the primary Br species at Etnean magmatic temperatures (in the 500-1100 °C temperature range and 0.1 MPa pressure; Aiuppa et al., 2005). The HBr output was unfortunately not determined during the 2006 eruption. If we assume the same mean HBr/SO₂ (7×10^{-4} by mass) as measured in 2004 (Aiuppa et al., 2005) then this yields a Br emission of 425 tons.

It is preferable to base the estimate on data from the actual 2006 eruption; however the percentage of BrO of the total emitted bromine is difficult to determine. BrO/SO₂ depends on factors including the plume age (distance from the vent, wind velocity), meteorology, time of day, etc (e.g., Bobrowski and Giuffrida, 2012). Observations and models suggest that BrO contents may represent 20 to ~50 % of total bromine within a few tens of minutes after plume release (von Glasow, 2010; Roberts et al., 2014). The total mass of bromine emitted during the 2006 Etna eruption would therefore be between 170 and 425 tons, which is comparable to

or larger than the mass of bromine in the pre-eruptive melt (125-141 tons, see above and SI), suggesting that Br was efficiently degassed from the basaltic melt.

Estimate of Br annual flux at Mount Etna

On the basis of the 2006 BrO gas monitoring data encompassing non-eruptive and eruptive periods (i.e., Aiuppa et al., 2005; Bobrowski et al., 2012), we calculate a time-averaged Br emission rate of 0.7 kt/yr (assuming that BrO = 40% of Br total, Oppenheimer et al., 2006; SI). This is similar to the estimate for the 2004 eruption from Aiuppa et al. (2005). However, as highlighted by Collins et al. (2009), the 2004 and 2006 eruptions were “gas-poor eruptions” thus 0.7 kt/yr should be considered as a minimum Br annual flux for Etna.

5.3.2 Bromine emission from an andesitic volcano: the 2010 Merapi plinian eruption

Merapi volcano (Java, Indonesia) is one of the most active and hazardous volcanoes in the world. The 2010 eruption (VEI 4; Solikhin et al., 2015) was the volcano’s largest since 1872. In contrast to the prolonged and effusive dome-forming eruptions typical of Merapi’s activity of the last decades, the 2010 eruption began explosively, before a new dome was rapidly emplaced. This new dome was subsequently destroyed by explosions, generating pyroclastic density currents. The initial explosive phase generated an ash plume that rose to 18 km altitude (Solikhin et al., 2015). The entire eruption released ~0.44 Tg of SO₂ (cumulative SO₂ output based on satellite observations; Surono et al., 2012), much more than previous Merapi eruptions (from 1992 to 2007; Surono et al., 2012). The SO₂ emission rates of the 2010 eruption greatly exceed background and eruptive emissions recorded at Merapi between 1986 and 2007 (Nho et al., 1996; Humaida et al., 2007; Surono et al., 2012). On the basis of the ‘petrological method’, Surono et al. (2012) and Preece et al. (2014) calculated that the magma volume needed to account for the amount SO₂ released is at least an order of magnitude higher than the estimated DRE volume of magma erupted. They inferred the existence of an

exsolved S-rich fluid phase in the pre-eruptive magma body, consistent with the conclusion given by Scaillet et al. (1998b, 2003) and Keppler (1999) to explain the common excess of sulfur upon explosive eruptions. According to VolatileCalc modelling by Preece et al. (2014), the vapour phase would have represented 1 wt% of the magma and degassing occurred in closed- (i.e., gas bubbles remained in physical contact and equilibrium with their host melt) rather than in open-system conditions prior to the explosive phase of the 2010 eruption.

The GOME-2 satellite instrument measured SO₂ SCD (slant column densities) of up to 8.9×10^{18} molecules.cm⁻² (paroxysmal phase of November 5, 2010; Hormann et al., 2013), while BrO/SO₂ ratios were extremely low (8×10^{-6} maximum), indicating that Br was virtually absent. Yet, considering a magma density of 2550 kg/m³, 55 wt% of phenocrysts (Preece et al., 2014) and an average Br content of 9 ppm in the melt inclusions (this study, Table A.2), 433 tons of Br were available in the pre-eruptive melt. In addition, if we consider the presence a free fluid phase in the reservoir (1 wt%; Preece et al., 2014) and the $D_{\text{Br}}^{\text{f/m}} = 9.1$ in andesitic melt (Fig. 2b), 73 tons of Br were stored in the fluid and hence immediately available during eruption. Note that we observe the same large discrepancy between the satellite-based estimate of the chlorine yield and the petrological one (see SI). In our opinion, the two most probable explanations are: (1) the paroxysmal phase of the eruption being ash-rich (opacity) and occurring in the middle of the night, the production of BrO was prevented until many hours later (as the reactions are UV-enabled) and is probably lower than in ash-poor plumes (2) satellite instruments measure gases which reached the stratosphere more effectively than those that remain lower in the atmosphere (significant amount of bromine might have been scavenged in the troposphere). Additional causes might include: (i) preferential S degassing owing to kinetic factors (e.g., Fiege et al., 2014), (ii) Br uptake by brine saturation during magma uprise, (iii) the involvement of other volatile species (e.g. CO₂) which may alter Br partitioning.

The case of Merapi 2010 eruption hints at the need of studies on Br speciation in ash-rich volcanic plumes and additional experimental constraints, in particular on the effect of volatiles other than H₂O on Br systematics.

5.3.3. Bromine emission during the cataclysmic Minoan eruption of Santorini volcano

The Late-Bronze age Minoan eruption discharged 38-86 km³ DRE of rhyodacitic magma (e.g. Pyle, 1990; Johnston et al., 2014). Petrological studies have shown that the pre-eruptive melt was rich in halogens, particularly in chlorine (2500-6000 ppm), and was most probably in equilibrium with an exsolved H₂O-Cl-rich fluid phase (Cadoux et al., 2014; Cadoux et al., 2015; Druitt et al., 2016). Here, we have measured for the first time the Br content of plagioclase-hosted melt inclusions from the Minoan plinian fallout deposit (Table A.2). They give an average value of 7.3 ± 0.8 ppm, which multiplied by the $D_{Br}^{f/m}$ of 20.2 (obtained in this study for a rhyodacitic composition at 900°C, 200 MPa and ~NNO; Fig. 3), indicate that the pre-eruptive fluid phase contained 147 ppm Br.

Assuming a minimum erupted volume of 39 km³ DRE and a magma crystallinity of 10%, the Minoan pre-eruptive melt would have contained 0.6 Mt of Br. Recent studies have shown that, in silicic magma systems, Br is efficiently degassed with water during eruption (Bureau et al., 2010; Cochain et al., 2015). If we assume that all the Br was degassed from the melt (i.e. we consider 0 ppm of Br in the interstitial melt), the Br output of the Minoan eruption was 0.6 Mt. If we add the contribution of the fluid phase (assuming that it represents 5 wt% of the magma mass, as in Cadoux et al., 2015), then the total Br output would have reached 1.3 Mt. These Br yields are consistent with previous estimates of 0.1-1.5 Mt (Cadoux et al., 2015) obtained by multiplying the chlorine yields by the mean molar Br/Cl ratio of 0.0022 of volcanic arc gases (Gerlach, 2004).

The estimated Br output of this single large explosive event (VEI 6-7) is > 100 times higher than the annual Br flux at a persistently degassing volcano such as the Etna (0.0007 Mt, see before) and the estimated global Br flux at volcanic arcs (0.005-0.015 Mt/yr; Pyle and Mather, 2009).

6. Conclusions

Determining halogen behaviour in magmatic systems is important to understand their role in the Earth's element cycles and to provide reliable constraints on the contribution of volcanism to atmospheric and ocean chemistry. The behaviour of the heavier halogens such as Br in magmatic systems is less well understood than that of Cl and F. We have experimentally determined the fluid/melt partitioning of bromine at shallow crustal pressure and temperature conditions (100-200 MPa, 900-1200°C) with mafic, intermediate and silicic natural melts. $D_{\text{Br}}^{\text{f/m}}$ values range from 5.0 ± 0.3 at 100 MPa – 1200°C for the basalt to 20.2 ± 1.2 at 200 MPa - 900°C for the rhyodacite. Our data confirm previous experimental constraints on synthetic model magma compositions (Bureau et al., 2000). They also show that $D_{\text{Br}}^{\text{f/m}}$ increases with increasing SiO₂ content of the melt (as for chlorine) and it also appears to be sensitive to melt temperature (increase of $D_{\text{Br}}^{\text{f/m}}$ as temperature decreases). These results suggest that the Br yield into atmosphere from relatively cold and silicic magmas will be much larger than that from hotter and more mafic magmas. The partition coefficients of this study will permit better estimates of the Br yield of past explosive eruptions, provided their pre-eruptive temperature is well known.

Our Br partition coefficient for Etna basalt, together with literature data on S and Cl behaviour, and S-Cl-Br volcanic gas compositions in mafic volcanic systems, allow first order quantitative modelling of S-Cl-Br degassing behaviour in shallow magma reservoirs, permitting a better interpretation of gas-monitoring data.

Acknowledgements

A.C. thanks N. Bouden (CRPG, Nancy) for his assistance during H₂O SIMS measurements, and S. Erdmann (ISTO, Orléans) who provided crystal mounts from Merapi andesite for melt inclusions analysis. A.C. is also grateful to Y. Missenard and P. Sarda (GEOPS, Orsay) for their help and discussion about error propagation. N. Metrich (IPGP, Paris) and A. Bertagnini (INGV, Pisa) provided melt inclusions from Stromboli. I. Di Carlo (ISTO, Orléans) and L. Brusca (INGV, Palermo) are acknowledged for their assistance with EMP and LA-ICPMS analyses, respectively. This work was partially supported by the ‘Laboratoire d’Excellence VOLTAIRE’ (University of Orléans, France), the French agency for research [ANR project #12-JS06-0009-01] and the European Research Council [ERC grant agreement n°305377]. A.A., T.A.M. and D.M.P. acknowledge the Diamond Light Source for time on Beamline I18 [Proposal sp8797]. We thank two anonymous reviewers for their insights on an earlier draft of this paper.

References

- Aiuppa, A., 2009. Degassing of halogens from basaltic volcanism: insights from volcanic gas observations. *Chemical Geology* 263, 99-109.
- Aiuppa, A., Giudice, G., Liuzzo, M., Tamburello, G., Allard, P., Calabrese, S., Chaplygin, I., McGonigle, A.J.S. and Taran, Y. 2012, First volatile inventory for Gorely volcano, Kamchatka, *Geophys. Res. Lett.* 39, L06307

766 Aiuppa, A., Baker, D.R., Webster, J.D., 2009. Halogens in volcanic systems. *Chemical*
767 *Geology* 263, 1-18.

768

769 Aiuppa, A., Federico, C., Franco, A., Giudice, G., Gurrieri, S., Inguaggiato, S., Liuzzo, M.,
770 McGonigle, A.J.S., Valenza, M., 2005. Emission of bromine and iodine from Mount Etna
771 volcano. *Geochemistry, Geophysics, Geosystems* 6.

772

773 Aiuppa, A., Federico, C., Paonita, A., Pecoraino, G., Valenza, M., 2002. S, Cl and F
774 degassing as an indicator of volcanic dynamics: the 2001 eruption of Mount Etna. *Geophys.*
775 *Res. Lett.* 29-11, doi 10.1029/2002GL015032.

776

777 Aiuppa, A., Giudice, G., Gurrieri, S., Liuzzo, M., Burton, M., Caltabiano, T., McGonigle,
778 A.J.S., Salerno, G., Shinohara, H., Valenza, M., 2008. Total volatile flux from Mount Etna.
779 *Geophysical Research Letters* 35, L24302, doi:24310.21029/22008GL035871.

780

781 Aiuppa, A., Moretti, R., Federico, C., Giudice, G., Gurrieri, S., Liuzzo, M., Papale, P.,
782 Shinohara, H., Valenza, M., 2007. Forecasting Etna eruptions by real-time observation of
783 volcanic gas composition. *Geology* 35, 1115–1118.

784

785 Allard, P., La Spina, A., Tamburello, G., Aiuppa, A., Burton, M., Di Muro, A., Staudacher, T.
786 (2011), First measurements of magmatic gas composition and fluxes during an eruption
787 (October 2010) of Piton de la Fournaise hot spot volcano, La Reunion Island. Abstract, 11th
788 Gas Workshop, Commission on the Chemistry of Volcanic Gases (CCVG)-IAVCEI-6, 2011-
789 09 Kamchatka, Russia

790

791 Alletti, M., 2008. Experimental investigation of halogen diffusivity and solubility in Etnean
792 basaltic melts. University of Palermo, Palermo, Italy, p. 92.
793

794 Alletti, M., Baker, D.R., Freda, C., 2007. Halogen diffusion in a basaltic melt. *Geochimica et*
795 *Cosmochimica Acta* 71, 3570-3580.
796

797 Alletti, M., Baker, D.R., Scaillet, B., Aiuppa, A., Moretti, R., Ottolini, L., 2009. Chlorine
798 partitioning between a basaltic melt and H₂O–CO₂ fluids at Mount Etna. *Chemical Geology*
799 263, 37-50.
800

801 Alletti, M., Burgisser, A., Scaillet, B., Oppenheimer, C., 2014. Chloride partitioning and
802 solubility in hydrous phonolites from Erebus volcano: A contribution towards a multi-
803 component degassing model. *GeoResJ* 3-4, 27-45.
804

805 Baker, D.R., Alletti, M., 2012. Fluid saturation and volatile partitioning between melts and
806 hydrous fluids in crustal magmatic systems: The contribution of experimental measurements
807 and solubility models. *Earth-Science Reviews* 114, 298-324.
808

809 Baker, D.R., Moretti, R., 2011. Modeling the Solubility of Sulfur in Magmas: A 50-Year Old
810 Geochemical Challenge, *Reviews in Mineralogy & Geochemistry*. Mineralogical Society of
811 America, pp. 167-213.
812

813 Beermann, O., 2010. The solubility of sulfur and chlorine in H₂O-bearing dacites of Krakatau
814 and basalts of Mt. Etna. *Leibniz Universität Hannover, Germany, Hannover*, p. 107.
815

816 Beermann, O., Botcharnikov, R.E., Nowak, M., 2015. Partitioning of sulfur and chlorine
817 between aqueous fluid and basaltic melt at 1050°C, 100 and 200 MPa. *Chemical Geology*
818 418, 132-157.

819

820 Behncke, B., Calvari, S., Giammanco, S., Neri, M., Pinkerton, H., 2008. Pyroclastic density
821 currents resulting from interaction of basaltic magma with hydrothermally altered rock: An
822 example from the 2006 summit eruptions of Mount Etna (Italy). *Bull. Volcanol.* 70, 1249–
823 1268, doi:1210.1007/s00445-00008-00200-00447.

824

825 Behncke, B., Falsaperla, S., Pecora, E., 2009. Complex magma dynamics at Mount Etna
826 revealed by seismic, thermal and volcanological data. *J. Geophys. Res.* 114, B03211,
827 doi:03210.01029/02008JB005882.

828

829 Bobrowski, N., Giuffrida, G., 2012. Bromine monoxide / sulphur dioxide ratios in relation to
830 volcanological observations at Mt. Etna 2006-2009. *Solid Earth* 3, 433-445.

831

832 Bobrowski, N., Hönninger, G., Galle, B., Platt, U., 2003. Detection of bromine monoxide in a
833 volcanic plume. *Nature* 423, 273–276.

834

835 Bobrowski, N., von Glasow, R., Giuffrida, G.B., Tedesco, D., Aiuppa, A., Yalire, M.,
836 Arellano, S., Johansson, M., Galle, B., 2015. Gas emission strength and evolution of the
837 molar ratio of BrO/SO₂ in the plume of Nyiragongo in comparison to Etna. *Journal of*
838 *Geophysical Research: Atmospheres* 120, 277-291.

839

840 Borodulin, G.P., Chevychelov, V.Y., Zaraysky, G.P., 2009. Experimental study of
841 partitioning of tantalum, niobium, manganese, and fluorine between aqueous fluoride fluid
842 and granitic and alkaline melts. *Doklady Earth Sciences* 427, 868-873.

843

844 Botcharnikov, R.E., Behrens, H., Holtz, F., Koepke, J., Sato, H., 2004. Sulfur and chlorine
845 solubility in Mt. Unzen rhyodacitic melt at 850°C and 200 MPa. *Chem Geol* 213, 207-225.

846

847 Botcharnikov, R.E., Holtz, F., Behrens, H., 2007. The effect of CO₂ on the solubility of H₂ O-
848 Cl fluids in andesitic melt. *Eur J Mineral* 19, 671-680.

849

850 Botcharnikov, R.E., Holtz, F., Behrens, H., 2015. Solubility and fluid-melt partitioning of
851 H₂O and Cl in andesitic magmas as a function of pressure between 50 and 500 MPa. *Chem*
852 *Geol*, doi:10.1016/j.chemgeo.2015.1007.1019.

853

854 Bureau, H., Auzende, A.L., Marocchi, M., Raepsaet, C., Munsch, P., Testemale, D., Mézouar,
855 M., Kubsky, S., Carrière, M., Ricolleau, A., Fiquet, G., 2016. Modern and past volcanic
856 degassing of iodine. *Geochimica et Cosmochimica Acta* 173, 114-125.

857

858 Bureau, H., Foy, E., Raepsaet, C., Somogyi, A., Munsch, P., Simon, G., Kubsky, S., 2010.
859 Bromine cycle in subduction zones through in situ Br monitoring in diamond anvil cells.
860 *Geochimica et Cosmochimica Acta* 74, 3839-3850.

861

862 Bureau, H., Keppler, H., Métrich, N., 2000. Volcanic degassing of bromine and iodine:
863 experimental fluid/melt partitioning data and applications to stratospheric chemistry. *Earth*
864 *and Planetary Science Letters* 183, 51-60.

865

866 Bureau, H., Métrich, N., 2003. An experimental study of bromine behaviour in water-
 867 saturated silicic melts. *Geochimica et Cosmochimica Acta* 67, 1689-1697.

868

869 Cadoux, A., Iacono-Marziano, G., Paonita, A., Deloule, E., Aiuppa, A., Eby, G.N., Costa, M.,
 870 Brusca, L., Berlo, K., Geraki, K., Mather, T.A., Pyle, D.M., Di Carlo, I., 2017. A new set of
 871 standards for in-situ measurement of bromine abundances in natural silicate glasses:
 872 application to SR-XRF, LA-ICP-MS and SIMS techniques. *Chemical Geology* 452, 60-70.

873

874 Cadoux, A., Scaillet, B., Bekki, S., Oppenheimer, C., Druitt, T.H., 2015. Stratospheric Ozone
 875 destruction by the Bronze-Age Minoan eruption (Santorini Volcano, Greece). *Scientific*
 876 *Reports* 5, 12243.

877

878 Cadoux, A., Scaillet, B., Druitt, T.H., Deloule, E., 2014. Magma storage conditions of large
 879 Plinian eruptions of Santorini Volcano (Greece). *Journal of Petrology* 55, 1129-1171.

880

881 Carroll, M.R., Webster, J.D., 1994. Solubilities of sulfur, noble gases, nitrogen, chlorine, and
 882 fluorine in magmas, in: Carroll, M.R., Holloway, J.R. (Eds.), *Volatiles in Magmas*.
 883 *Mineralogical Society of America*, pp. 231-279.

884

885 Chevychelov, V.Y., Bocharnikov, R.E., Holtz, F., 2008a. Experimental study of chlorine and
 886 fluorine partitioning between fluid and subalkaline basaltic melt. *Doklady Earth Sciences* 422,
 887 1089–1092.

888

889 Chevychelov, V.Y., Botcharnikov, R.E., Holtz, F., 2008b. Partitioning of Cl and F between
890 fluid and hydrous phonolitic melt of Mt. Vesuvius at 850-1000 °C and 200 MPa. *Chem. Geol.*
891 256, 172–184.

892

893 Cochain, B., Sanloup, C., de Grouchy, C., Crépisson, C., Bureau, H., Leroy, C., Kantor, I.,
894 Irifune, T., 2015. Bromine speciation in hydrous silicate melts at high pressure. *Chemical*
895 *Geology* 404, 18-26.

896

897 Collins, S.J., Pyle, D.M., MacLennan, J., 2009. Melt inclusions track pre-eruption storage and
898 dehydration of magmas at Etna. *Geology* 37, 571–574.

899

900 Costa, F., Andreastuti, S., Bouvet de Maisonneuve, C., Pallister, J.S., 2013. Petrological
901 insights into the storage conditions, and magmatic processes that yielded the centennial 2010
902 Merapi explosive eruption. *Journal of Volcanology and Geothermal Research* 261, 209-235.

903

904 Daniel, J.S., Solomon, S., Portmann, R.W., Garcia, R.R., 1999. Stratospheric ozone
905 destruction: The importance of bromine relative to chlorine. *J. Geophys. Res.* 104, 23871–
906 23880.

907

908 de Chambost, E., Schumacher, M., Lovestam, G., Claesson, S., 1996. Achieving high
909 transmission with the Cameca IMS 1270, in: Benninghoven, A., Hagenhoff, B., Werner, H.W.
910 (Eds.), *Secondary Ion Mass Spectrometry, SIMS X*. Wiley, Chichester, pp. 1003-1006.

911

912 Di Carlo, I., Pichavant, M., Rotolo, S.G., Scaillet, B., 2006. Experimental crystallization of a
 913 high-K arc basalt: the golden pumice, Stromboli volcano (Italy). *Journal of Petrology* 47,
 914 1317-1343.
 915
 916 Dolejs, D., Baker, D.R., 2007a. Liquidus equilibria in the system K_2O - Na_2O - Al_2O_3 - SiO_2 -
 917 F_2O_{-1} - H_2O to 100 MPa: I. Silicate fluoride liquid immiscibility in anhydrous systems. *J*
 918 *Petrol* 48, 785-806.
 919
 920 Dolejs, D., Baker, D.R., 2007b. Liquidus equilibria in the system K_2O - Na_2O - Al_2O_3 - SiO_2 -
 921 F_2O_{-1} - H_2O to 100 MPa: II. Differentiation paths of fluorosilicic magmas in hydrous
 922 systems. *J Petrol* 48, 807-828.
 923
 924 Druitt, T.H., Mercier, M., Florentin, L., Deloule, E., Cluzel, N., Flaherty, T., Médard, E.,
 925 Cadoux, A., 2016. Magma Storage and Extraction Associated with Plinian and Interplinian
 926 Activity at Santorini Caldera (Greece). *Journal of Petrology* 57, 461-494.
 927
 928 Edmonds, M., Gerlach, T.M., Herd, R.A., 2009. Halogen degassing during ascent and
 929 eruption of water-poor basaltic magma. *Chemical Geology* 263, 122-130.
 930
 931 Ferlito, C., Viccaro, M., Nicotra, E., Cristofolini, R., 2010. Relationship between the flank
 932 sliding of the South East Crater (Mt. Etna, Italy) and the paroxysmal event of November 16,
 933 2006. *Bulletin of Volcanology* 72, 1179-1190.
 934
 935 Fiege, A., Behrens, H., Holtz, F. and Adams, F. (2014) Kinetic vs. thermodynamic control of
 936 degassing of H_2O - S - Cl -bearing andesitic melts. *Geochim. Cosmochim. Acta* 125, 241-264.

937 Foustoukos, D.I., Seyfried, W.E., 2007. Trace element partitioning between vapor, brine and
 938 halite under extreme phase separation conditions. *Geochim. Cosmochim. Acta* 71, 2056–
 939 2071.

940

941 Gaillard, F., Scaillet, B., 2014. A theoretical framework for volcanic degassing chemistry in a
 942 comparative planetology perspective and implications for planetary atmospheres. *Earth and*
 943 *Planetary Science Letters* 403, 307-316.

944

945 Gennaro M.E. (2017). Sulfur behavior and redox conditions in Etnean hydrous basalts
 946 inferred from melt inclusions and experimental glasses. PhD thesis. Università degli Studi di
 947 Palermo.

948

949 Gerlach, T.M., 2004. Volcanic sources of tropospheric ozone-depleting trace gases.
 950 *Geochemistry, Geophysics, Geosystems* 5, Q09007.

951

952 Hörmann, C., Sihler, H., Bobrowski, N., Beirle, S., Penning de Vries, M., Platt, U., Wagner,
 953 T., 2013. Systematic investigation of bromine monoxide in volcanic plumes from space by
 954 using the GOME-2 instrument. *Atmos. Chem. Phys.* 13, 4749-4781.

955

956 Humaida, H., Sumarti, S., Subandriyo, Nandaka, A., Sukarnen, I.G.M., Suharno, Rinekso, K.,
 957 Badrijas, Ismai, Sunarto, 2007. Aktivitas Merapi 2006 dan Pemantauan Emisi SO₂ dengan
 958 COSPEC, in *Erupsi Merapi 2006. Laporan dan Kajian Vulkanisme Erupsi 2006*. Departement
 959 Energi dan Sumber Daya Mineral, Badan Geologi, Pusat Vulkanologi dan Mitigasi Bencana
 960 Geologi.

961

962 Iacono-Marziano, G., Morizet, Y., Le Trong, E., Gaillard, F., 2012. New experimental data
 963 and semi-empirical parameterization of H_2O - CO_2 solubility in mafic melts. *Geochimica et*
 964 *Cosmochimica Acta* 97, 1-23.

965

966 Johnston, E.N., Sparks, R.S.J., Phillips, J.C., Carey, S., 2014. Revised estimates for the
 967 volume of the late Bronze Age Minoan eruption, Santorini. *Journal of the Geological Society,*
 968 *London*, 171, 583-590.

969

970 Jugo, P.J., Wilke, M., Botcharnikov, R.E., 2010. Sulfur K-edge XANES analysis of natural
 971 and synthetic basaltic glasses: implications for S-speciation and S content as function of
 972 oxygen fugacity. *Geochim. Cosmochim. Acta* 74, 5926–5938.

973

974 Kahl, M., Chakraborty, S., Pompilio, M., Costa, F., 2015. Constraints on the Nature and
 975 Evolution of the Magma Plumbing System of Mt. Etna Volcano (1991-2008) from a
 976 Combined Thermodynamic and Kinetic Modelling of the Compositional Record of Minerals.
 977 *Journal of Petrology* 56, 2025-2068.

978

979 Kendrick, M.A., Arculus, R.J., Danyushevsky, L.V., Kamenetsky, V.S., Woodhead, J.D.,
 980 Honda, M., 2014. Subduction-related halogens (Cl, Br and I) and H_2O in magmatic glasses
 981 from Southwest Pacific Backarc Basins. *Earth and Planetary Science Letters* 400, 165-176.

982

983 Keppler, H. (1999) Experimental Evidence for the Source of Excess Sulfur in Explosive
 984 Volcanic Eruptions. *Science* 284, 1652-1654.

985

986 Khalil, M.A.K., Rasmussen, R.A., Gunawardena, R., 1993. Atmospheric methyl bromide:
 987 Trends and global mass balance. *Journal of Geophysical Research: Atmospheres* 98, 2887-
 988 2896.
 989
 990 Kutterolf, S., Hansteen, T.H., Appel, K., Freundt, A., Krüger, K., Pérez, W., Wehrmann, H.,
 991 2013. Combined bromine and chlorine release from large explosive volcanic eruptions: A
 992 threat to stratospheric ozone? *Geology* 41, 707–710.
 993
 994 Lesne, P., Scaillet, B., Pichavant, M., 2015. The solubility of sulfur in hydrous basaltic melts.
 995 *Chemical Geology* 418, 104-116.
 996
 997 Lesne, P., Scaillet, B., Pichavant, M., Beny, J.-M., 2011b. The carbon dioxide solubility in
 998 alkali basalts: an experimental study. *Contributions to Mineralogy and Petrology* 162, 153-
 999 168.
 1000
 1001 Lesne, P., Scaillet, B., Pichavant, M., Iacono-Marziano, G., Beny, J.-M., 2011a. The H₂ O
 1002 solubility of alkali basaltic melts: an experimental study. *Contributions to Mineralogy and*
 1003 *Petrology* 162, 133-151.
 1004
 1005 Longerich, H.P., Jackson, S.E., Fryer, B.J., Strong, D.F., 1993. The laser ablation microprobe
 1006 inductively coupled plasma-mass spectrometer. *Geoscience Canada* 20, 21-27.
 1007
 1008 Manó, S., Andreae, M.O., 1994. Emission of Methyl Bromide from Biomass Burning.
 1009 *Science* 263, 1255.
 1010

1011 Martel, C., Pichavant, M., Holtz, F., Scaillet, B., Bourdier, J.-L., Traineau, H., 1999. Effects
 1012 of fO_2 and H_2O on andesite phase relations between 2 and 4 kbar. *J. Geophys. Res.* 104,
 1013 29,453–429,470.

1014

1015 Martin, R.S., Roberts, T.J., Mather, T.A., Pyle, D.M., 2009. The implications of H_2S and H_2
 1016 stability in high-T mixtures of magmatic and atmospheric gases for the production of oxidized
 1017 trace species (e.g., BrO and NO_x). *Chem. Geol.* 263, 143–150.

1018

1019 Mather, T.A., 2015. Volcanoes and the environment: Lessons for understanding Earth's past
 1020 and future from studies of present-day volcanic emissions. *Journal of Volcanology and*
 1021 *Geothermal Research* 304, 160-179.

1022

1023 Mather, T.A., Witt, M.L.I., Pyle, D.M., Quayle, B.M., Aiuppa, A., Bagnato, E., Martin, R.S.,
 1024 Sims, K.W.W., Edmonds, M., Sutton, A.J., Ilyinskaya, E., 2012. Halogens and trace metal
 1025 emissions from the ongoing 2008 summit eruption of Kīlauea volcano, Hawaii *Geochimica et*
 1026 *Cosmochimica Acta* 83, 292-323.

1027

1028 Métrich, N., Allard, P., Spilliarde, N., Andronico, D., Burton, M., 2004. 2001 flank eruption
 1029 of the alkali- and volatile-rich primitive basalt responsible for Mount Etna's evolution in the
 1030 last three decades. *Earth and Planetary Science Letters* 228, 1–17.

1031

1032 Métrich, N., Bertagnini, A., Di Muro, A., 2010. Conditions of magma storage, degassing and
 1033 ascent at Stromboli: new insights into the volcano plumbing system with inferences on the
 1034 eruptive dynamics. *J. Petrol.* 51, 603-626.

1035

1036 Métrich, N., Bertagnini, A., Landi, P., Rosi, M., 2001. Crystallisation driven by
 1037 decompression and water loss at Stromboli volcano (Aeolian Islands). *J. Petrol.* 42, 1471-
 1038 1490.

1039

1040 Métrich, N., Deloule, E., 2014. Water content, δD and $\delta^{11}B$ tracking in the Vanuatu arc
 1041 magmas (Aoba Island): Insights from olivine-hosted melt inclusions. *Lithos* 206-207, 400-
 1042 408.

1043

1044 Métrich, N., Wallace, P., 2008. Volatile abundances in basaltic magmas and their degassing
 1045 paths tracked by melt inclusions, in: Putirka, K., Tepley, F. (Eds.), *Minerals, Inclusions and*
 1046 *Volcanic Processes*. Mineralogical Society of America, pp. 363-402.

1047

1048 Montzka, S., and Reimann, S. (Coordinating Lead Authors), Engel, A., Krüger, K.,
 1049 O'Doherty, S., Sturges, W.T., Blake, D., Dorf, M., Fraser, P., Froidevaux, L., Jucks, K.,
 1050 Kreher, K., Kurylo, M.J., Mellouki, A., Miller, J., Nielsen, O.-J., Orkin, V.L., Prinn, R.G.,
 1051 Rhew, R., Santee, M.L., Stohl, A., and Verdonik, D., Ozone-depleting substances (ODSs) and
 1052 related chemicals, Chapter 1 in *Scientific Assessment of Ozone Depletion: 2010*, Global
 1053 Ozone Research and Monitoring Project–Report No. 52, 516 pp., World Meteorological
 1054 Organization, Geneva, Switzerland, 2011.

1055

1056 Moretti, R., Ottonello, G., 2005. Solubility and speciation of sulfur in silicate melts: The
 1057 Conjugated Toop-Samis-Flood-Grjotheim (CTSFG) model. *Geochimica et Cosmochimica*
 1058 *Acta* 69, 801-823.

1059

1060 Mungall, J.E. and Brenan, J.M. (2003) Experimental evidence for the chalcophile behavior of
 1061 the halogens. *Can. Mineral.* 41, 207-220.

1062

1063 Neri, M., Behncke, B., Burton, M., Galli, G., Giammanco, S., Pecora, E., Privitera, E.,
 1064 Reitano, D., 2006. Continuous soil radon monitoring during the July 2006 Etna eruption.
 1065 *Geophys. Res. Lett.* 33, L24316, doi: 24310.21029/22006GL028394.

1066

1067 Nho, E.-Y., Le Cloarec, M.-F., Ardouin, B., Tjetjep, W.S., 1996. Source strength assessment
 1068 of volcanic trace elements emitted from the Indonesian Arc. *Journal of Volcanology and*
 1069 *Geothermal Research* 74, 121–129.

1070

1071 Oppenheimer, C., Tsanev, V.I., Braban, C.F., Cox, R.A., Adams, J.W., Aiuppa, A.,
 1072 Bobrowski, N., Delmelle, P., Barclay, J., McGonigle, A.J.S., 2006. BrO formation in volcanic
 1073 plumes. *Geochimica et Cosmochimica Acta* 70, 2935-2941.

1074

1075 Preece, K., Gertisser, R., Barclay, J., Berlo, K., Herd, R.A., 2014. Pre- and syn-eruptive
 1076 degassing and crystallisation processes of the 2010 and 2006 eruptions of Merapi volcano,
 1077 Indonesia. *Contributions to Mineralogy and Petrology* 168, 1061.

1078

1079 Pyle, D.M., 1990, New volume estimates for the Minoan eruption, In: *Thera and the Aegean*
 1080 *World III*, vol 2, eds. D Hardy, J. Keller, VP Galanopoulos, NC Flemming and TH Druitt, pp
 1081 113-121; The Thera Foundation, London.

1082

1083 Pyle, D.M., Mather, T.A., 2009. Halogens in igneous processes and their fluxes to the
 1084 atmosphere and oceans from volcanic activity: A review. *Chemical Geology* 263, 110-121.

1085

1086 Kravchuk, F., Keppler, H., 1994. Distribution of chloride between aqueous fluids and felsic
 1087 melts at 2 kbar and 800°C. *Eur. J. Mineral.* 6, 913-923.

1088

1089 Roberts, T.J., Braban, C.F., Martin, R.S., Oppenheimer, C., Adams, J.W., Cox, R.A.,
 1090 Griffiths, P.T., 2009. Modelling reactive halogen formation and ozone depletion in volcanic
 1091 plumes. *Chemical Geology* 263, 151-163.

1092

1093 Roberts, T.J., Martin, R.S., Jourdain, L., 2014. Reactive bromine chemistry in Mount Etna's
 1094 volcanic plume: the influence of total Br, high-temperature processing, aerosol loading and
 1095 plume–air mixing. *Atmospheric Chemistry and Physics* 14, 11201-11219.

1096

1097 Sawyer, G.M., Salerno, G.G., Le Blond, J.S., Martin, R.S., Spampinato, L., Roberts, T.J.,
 1098 Mather, T.A., Witt, M.L.I., Tsanev, V.I. and Oppenheimer, C. 2011, Gas and aerosol
 1099 emissions from Villarrica volcano, Chile, *J. Volcanol. Geotherm. Res.* 203, 62-75.

1100

1101 Scaillet, B., Holtz, F., Pichavant, M., 1998a. Phase equilibrium constraints on the viscosity of
 1102 silicic magmas: 1. Volcanic-plutonic comparison. *Journal of Geophysical Research: Solid*
 1103 *Earth* 103, 27257-27266.

1104

1105 Scaillet, B., Clément, B., Evans, B. W., & Pichavant, M. 1998b. Redox control of sulfur
 1106 degassing in silicic magmas. *Journal of Geophysical Research: Solid Earth*, 103(B10),
 1107 23937-23949.

1108

1109 Scaillet, B., Evans, B.W., 1999. The 15 June 1991 Eruption of Mount Pinatubo. I. Phase
 1110 Equilibria and Pre-eruption P-T-f O₂ -f H₂ O Conditions of the Dacite Magma. *Journal of*
 1111 *Petrology* 40, 381-411.
 1112
 1113 Scaillet, B., Luhr, J. F., & Carroll, M. R. 2003. Petrological and volcanological constraints on
 1114 volcanic sulfur emissions to the atmosphere. *Volcanism and the Earth's Atmosphere*, AGU
 1115 Monograph 139, 11-40.
 1116
 1117 Seo, J.H., Zajacz, Z., 2016. Fractionation of Cl/Br during fluid phase separation in magmatic–
 1118 hydrothermal fluids. *Geochim. Cosmochim. Acta* 183, 125–137.
 1119
 1120 Shannon, R.D., 1976. Revised effective ionic radii and systematic studies of interatomic
 1121 distances in halides and chalcogenides. *Acta Cryst. A* 32, 751-767.
 1122
 1123 Shishkina, T.A., Botcharnikov, R.E., Holtz, F., Almeev, R.R., Portnyagin, M.V., 2010.
 1124 Solubility of H₂ O- and CO₂ -bearing fluids in tholeiitic basalts at pressures up to 500 MPa.
 1125 *Chemical Geology* 277, 115-125.
 1126
 1127 Signorelli, S., Carroll, M.R., 2000. Solubility and fluid-melt partitioning of Cl in hydrous
 1128 phonolitic melts. *Geochimica et Cosmochimica Acta* 64, 2851-2862.
 1129
 1130 Solikhin, A., Thouret, J.-C., Liew, S.C., Gupta, A., Sayudi, D.S., Oehler, J.-F., Kassouk, Z.,
 1131 2015. High-spatial-resolution imagery helps map deposits of the large (VEI 4) 2010 Merapi
 1132 Volcano eruption and their impact. *Bulletin of Volcanology* 77, 20.
 1133

1134 Spilliaert, N., Metrich, N., Allard, P., 2006. S-Cl-F degassing pattern of water rich alkali
 1135 basalt: modelling and relationship with eruption styles of Mount Etna volcano. *Earth Planet.*
 1136 *Sci. Lett.* 248, 772-786.
 1137
 1138 Stelling, J., Botcharnikov, R.E., Beermann, O., Nowak, M., 2008. Solubility of H₂O- and
 1139 chlorine-bearing fluids in basaltic melt of Mount Etna at T = 1050-1205°C and P = 200 MPa.
 1140 *Chemical Geology* 256, 102-110.
 1141
 1142 Surono, Jousset, P., Pallister, J., Boichu, M., Buongiorno, M.F., Budisantoso, A., Costa, F.,
 1143 Andreastuti, S., Prata, F., Schneider, D., Clarisse, L., Humaida, H., Sumarti, S., Bignami, C.,
 1144 Griswold, J., Carn, S., Oppenheimer, C., Lavigne, F., 2012. The 2010 explosive eruption of
 1145 Java's Merapi volcano - A '100-year' event. *Journal of Volcanology and Geothermal Research*
 1146 241-242, 121-135.
 1147
 1148 von Glasow, R., 2010. Atmospheric chemistry in volcanic plumes. *Proceedings of the*
 1149 *National Academy of Sciences* 107, 6594-6599, doi:6510.1073/pnas.0913164107.
 1150
 1151 von Glasow, R., Bobrowski, N., Kern, C., 2009. The effects of volcanic eruptions on
 1152 atmospheric chemistry. *Chemical Geology* 263, 131-142.
 1153
 1154 Warwick, N.J., Pyle, J.A., Carver, G.D., Yang, X., Savage, N.H., O'Connor, F.M., Cox, R.A.,
 1155 2006. Global modeling of biogenic bromocarbons. *J. Geophys. Res.* 111, D24305,
 1156 doi:24310.21029/22006JD007264.
 1157

1158 Webster, J.D., 1990. Partitioning of F between H₂O and CO₂ fluids and topaz rhyolite melt.
 1159 Contrib Mineral Petrol 104, 424-438.
 1160
 1161 Webster, J.D., 1992a. Water solubility and chlorine partitioning in Cl-rich granitic systems:
 1162 Effects of melt composition at 2 kbar and 800°C. *Geochimica et Cosmochimica Acta* 56, 679-
 1163 687.
 1164
 1165 Webster, J.D., 1992b. Fluid–melt interactions involving Cl-rich granites: experimental study
 1166 from 2 to 8 kbar. *Geochimica et Cosmochimica Acta* 56, 679–687.
 1167
 1168 Webster, J.D., 2004. The exsolution of magmatic hydrosaline melts. *Chem Geol* 210, 33-48.
 1169
 1170 Webster, J.D., Holloway, J.R., 1990. Partitioning of F and Cl between hydrothermal fluids
 1171 and highly evolved granitic magmas, in: Stein, H.J., Hannah, J.L. (Eds.), *Ore-bearing granite*
 1172 *systems: Petrogenesis and mineralizing processes*. Geological Society of America Special
 1173 Paper, pp. 21-34.
 1174
 1175 Webster, J.D., Kinzler, R.J., Mathez, E.A., 1999. Chloride and water solubility in basalt and
 1176 andesite melts and implications for magmatic degassing. *Geochimica et Cosmochimica Acta*
 1177 63, 729-738.
 1178
 1179 Webster, J.D., De Vivo, B., Tappen, C., 2003. Volatiles, magmatic degassing and eruptions of
 1180 Mt. Somma-Vesuvius: constraints from silicate melt inclusions, solubility experiments and
 1181 modeling, in: De Vivo, B., Bodnar, R.J. (Eds.), *Melt Inclusions in Volcanic Systems:*
 1182 *Methods, Applications and Problems*. Dev Volcanol Elsevier, Amsterdam, pp. 207-226.

1183

1184 Webster, J.D., Tappen, C.M., Mandeville, C.W., 2009. Partitioning behavior of chlorine and
 1185 fluorine in the system apatite-melt-fluid. II: Felsic silicate systems at 200 MPa. *Geochimica et*
 1186 *Cosmochimica Acta* 73, 559-581.

1187

1188 Webster, J.D., Goldoff, B., Sintoni, M.F., Shimizu, N., De Vivo, B., 2014. C-O-H-Cl-S-F
 1189 volatile solubilities, partitioning, and mixing in phonolitic-trachytic melts and aqueous-
 1190 carbonic vapor \pm saline liquid at 200 MPa. *J Petrol* 55, 2217-2248.

1191

1192 Webster, J.D., Vetere, F., Botcharnikov, R.E., Goldoff, B., McBirney, A., Doherty, A.L.,
 1193 2015. Experimental and modeled chlorine solubilities in aluminosilicate melts at 1 to 7000
 1194 bars and 700 to 1250 °C: Applications to magmas of Augustine Volcano, Alaska. *American*
 1195 *Mineralogist* 100, 522-535.

1196

1197 Webster, J.D., Baker, D.R., Aiuppa, A., 2018. Halogens in Mafic and Intermediate-silica
 1198 Content Magmas, in: Harlow, D., Aranovich, L.Y. (Eds.), *The Role of Halogens in Terrestrial*
 1199 *and Extraterrestrial Geochemical Processes: Surface, Crust, and Mantle*. Springer
 1200 International Publishing, pp. VI, 1030.

1201

1202 Witt, M. L. I., T. A. Mather, D. M. Pyle, A Aiuppa, E. Bagnato, and V. I. Tsanev (2008),
 1203 Mercury and halogen emissions from Masaya and Telica volcanoes, Nicaragua, *J. Geophys.*
 1204 *Res.*, 113, B06203, doi:10.1029/2007JB005401

1205

1206 Zajacz, Z., Candela, P.A., Piccoli, P.M., Sanchez-Valle, C., 2012. The partitioning of sulfur
1207 and chlorine between andesite melts and magmatic volatiles and the exchange coefficients of
1208 major cations. *Geochim Cosmochim Acta* 89, 81-101.

Figure Captions

Figure 1. Partitioning of bromine between melt and fluid in the run products at 1200°C, 100 MPa and $fO_2 \sim NNO$. The $D_{Br}^{f/m}$ of the basaltic composition, determined by linear regression through the origin, is: 4.95 ± 0.33 . The error on the partition coefficient corresponds to the error on the slope of the regression line, as determined by the least squares method.

Figure 2. (a) Melt Br contents versus bulk Br contents (ppm) for the andesitic and rhyodacitic compositions at 1060°C, 200 MPa and $fO_2 \sim NNO$. **(b)** and **(c)** Partitioning of bromine between melt and fluid in the andesitic and rhyolitic run products, respectively, at those conditions. The $D_{Br}^{f/m}$ determined by linear regression through the origin are: 9.1 ± 0.6 for the andesite and 14.0 ± 0.6 for the rhyodacite. The errors on $D_{Br}^{f/m}$ are the errors on the regression lines slope, see Figure 1 caption.

Figure 3. Partitioning of bromine between melt and fluid for the rhyodacitic composition, at 900°C, 200 MPa, $\sim NNO$. At lower temperature, the $D_{Br}^{f/m}$ of the rhyodacite increases: 20.2 ± 1.2 . Error on $D_{Br}^{f/m}$: see Figure 1 caption. The results are consistent with those of Bureau et al. (2000) on synthetic albitic composition.

Figure 4. $D_{Br}^{f/m}$ as a function of SiO_2 (wt%) of the run products of this study. The data for the 900°C – 200 MPa experiment of Bureau et al. (2000) is also plotted. This figure shows the effect of melt composition on $D_{Br}^{f/m}$ and also suggests an effect of the temperature, at least for the more silicic melts.

Figure 5. $D_{Br}^{f/m}$ of the rhyodacite composition versus partition experiment temperature (°C).

Data at 900°C and 1060°C are at 200 MPa and data at 1200°C is at 100 MPa.

Figure 6. (a) Triangular plot of S-Cl-Br*300 compositions of volcanic gas samples from selected mafic arc volcanoes. All data refer to near-vent in-situ measurements with filter packs, and are thus representative of gas species SO₂, HCl and HBr (the main S and halogen reservoirs in near-vent plumes, Aiuppa et al., 2005). Volcanic gas data sources: Reunion Island (Indian Ocean): Allard et al (2011); Nyiragongo (Congo): Bobrowski et al. (2015); Hawaii (Pacific Ocean): Mather et al., (2012); Etna (Sicily): Aiuppa et al. (2005), Aiuppa, (2009), Aiuppa, unpublished results; Stromboli (Aeolian Islands): Aiuppa, (2009); Masaya (Nicaragua): Witt et al, (2008); Mount Asama (Japan): Aiuppa, (2009), Aiuppa, unpublished results; Myike-jima (Japan): Aiuppa, (2009), Aiuppa, unpublished results; Gorely (Kamchatka, Russia): Aiuppa et al. (2012); Villarrica (Chile): Sawyer et al., (2011). For comparison, the model-derived compositions of gas initially coexisting with an Etna-like primitive melt (S: 0.27 wt.%, Cl: 0.18 wt.%, and Br: 5.1 ppm) are shown by the thick solid green curve. Dashed green lines are examples of Etna-like melt model trends obtained using same initial S and Cl contents (S: 0.27 wt.%, Cl: 0.18 wt.%) but slightly different initial Br contents (of respectively 3 and 6.1 ppm), within the range observed in glass inclusions (see Table A.2). The initial Br contents for the 3 Etna runs are labeled in the plot. Model lines are obtained using the Rayleigh-type open-system equations described in the text. Extent of degassing along both model lines varies from top (“early gas”) to bottom (“late gas”) (R values for specific points are shown in italics). See text for discussion. **(b)** The glass inclusion compositions from Etna and Stromboli (data from Table A.2) are displayed against the model-derived compositions, ranging from S-rich “*early melts*” to halogen-enriched (relative to S) “*late melts*”. The melt model line (solid red curve) is derived from the same Etna-like

1258 primitive melt composition given above (S: 0.27 wt.%, Cl: 0.18 wt.%, and Br: 5.1 ppm).
1259 Dashed red lines are examples of Etna-like melt model trends obtained using same initial S
1260 and Cl contents (S: 0.27 wt.%, Cl: 0.18 wt.%) but slightly different initial Br contents (of
1261 respectively 3 and 6.1 ppm), within the range observed in glass inclusions (see Table A.2).
1262 The initial Br contents for the 3 Etna runs are labeled in the plot. The melt model trend
1263 initialized at conditions representative of a Stromboli's primitive melt (S: 0.2 wt.%, Cl: 0.17
1264 wt.%, and Br: 4.8 ppm; see Table A.2) is depicted by the orange solid line. R values for
1265 specific points are shown in italics.

1266

1267 **Table Captions**

1268

1269 **Table 1.** Major element composition of the starting dry glasses used for the partitioning
1270 experiments.

1271

1272 **Table 2.** Results of the fluid/melt partitioning experiments.

1273

1274 **Table 3.** Major element composition (wt%) of the partition experiment products.

Table 1. Major element composition of the starting dry glasses used for the partitioning experiments

Volcano: Eruption	Etna: 11/22/2002		Santorini: USC-2		Santorini: Minoan	
Sample name	ET02PA27 ^a		S09-22 ^b		S82-30 ^c	
<i>Major oxides (wt%)</i>	<i>n = 32</i>	$\pm 1\sigma$	<i>n = 8</i>	$\pm 1\sigma$	<i>n = 22</i>	$\pm 1\sigma$
SiO ₂	47.95	0.82	58.88	0.43	71.24	0.26
TiO ₂	1.67	0.11	1.28	0.05	0.45	0.04
Al ₂ O ₃	17.32	0.27	16.16	0.17	14.87	0.15
FeO _{tot}	10.24	0.13	8.18	0.25	2.85	0.18
MnO	nd	nd	0.20	0.09	0.08	0.05
MgO	5.76	0.28	2.77	0.09	0.73	0.05
CaO	10.93	0.37	6.46	0.12	2.34	0.14
Na ₂ O	3.45	0.16	4.07	0.15	4.24	0.08
K ₂ O	1.99	0.10	1.67	0.06	3.08	0.11
P ₂ O ₅	0.51	0.12	0.31	0.06	0.13	0.04
Original sum	99.82		96.66		98.40	

Major element analyses performed by electron microprobe

a: from Iacono-Marziano et al. (2012)

b: from Cadoux et al. (2017), recalculated to 100%

c: from Cadoux et al. (2014, 2017), recalculated to 100%

n: number of analyses, and σ : standard deviation of the average of *n* analyses

nd: not determined

These dry glasses were also used to synthesize Br standards characterized in Cadoux et al. (2017)

Table 2. Results of the fluid/melt partitioning experiments

	[Br ^o] ^a (ppm)	fluid/melt mass ratio	[Br] _{melt} ^b (ppm)	± 1σ	[H ₂ O] _{melt} ^c (wt%)	± 1σ	[Br] _{fluid} ^d (ppm)	± error (ppm)	D _{Br} ^{f/m}	± error
Experiment #1: Au-Pd capsule, 1200°C, 100 MPa, ~NNO (pH₂ = 2 bars), 24 hours										
Run product # (B for basalt)										
M1-B	72181	0.06	3753	168	n.d.		14298	1595 8	3.8	4.3
Experiment #2: Au-Pd capsule, 1200°C, 100 MPa, ~NNO (pH₂ = 2 bars), 24 hours										
M2-B	14251 5	0.08	9112	464	n.d.		47027	1265 7	5.2	1.4
Experiment #3: Au-Pd capsules, 1200°C, 100 MPa, ~NNO (pH₂ = 2 bars), 24 hours										
Run product # (B for basalt, A for andesite, RD for rhyodacite)										
M3-B	24222	0.12	2034	290	3.4	0.0	9370	3845	4.6	2.0
M3-A	24222	0.12	1912	376	4.8	0.1	12298	6227	6.4	3.5
M3-RD	24222	0.12	1426	42	2.9	0.0	16065	1073	11.3	0.9
Experiment #4: Au-Pd capsules, 1060°C, 200 MPa, ~NNO (pH₂ = 2 bars), 48 hours										
M4-A1	999	0.11	69.5	0.1	7.2	0.1	948	138	13.7	2.0
M4-A2	4968	0.11	359	48	7.3	0.1	4439	1498	12.3	4.5
M4-A3	9874	0.11	733	79	7.3	0.2	8396	2462	11.5	3.6
M4-A4	24222	0.12	1960	34	7.2	0.1	16908	2499	8.6	1.3
M4-RD1	999	0.11	69	10	5.2	0.1	662	204	9.3	3.3
M4-RD2	4968	0.11	240	82	4.9	0.2	4968	1437	20.6	9.3
M4-RD3	9874	0.11	591	24	5.4	0.3	8626	966	14.6	1.8
M4-RD4	24222	0.12	1483	242	5.1	0.1	20314	4418	13.7	3.8
Experiment #5: Au capsules, 900°C, 200 MPa, ~NNO (pH₂ = 2 bars), 92 hours										
M5-RD1	999	0.12	79	6	6.8	0.4	701	162	8.6	2.2
M5-RD2	4968	0.11	226	31	6.0	0.3	6307	981	27.9	5.9
M5-RD3	9874	0.11	608	97	6.5	0.5	10113	2704	16.6	5.2
M5-RD4	24222	0.11	1251	214	5.6	0.1	26037	4452	20.8	5.1

Uncertainties on T and P are ± 10°C and ± 2 MPa, respectively.

a: calculated Br content loaded into capsule in H₂O+NaBr solution

b: measured by LA-ICP-MS in run-product glasses from experiments #1 and 2 (average of 3 to 10 analyses per charge), by SIMS in glasses from experiments #3 to 5 (3-6 analyses per charge)

c: H₂O content determined by SIMS (5-7 analyses per charge) in run-product glasses from exp. #3 to 5. H₂O_{melt} was not measured in run products from exp. #1 and 2.

d: calculated by mass balance (see supplementary material for details)

1275

1276

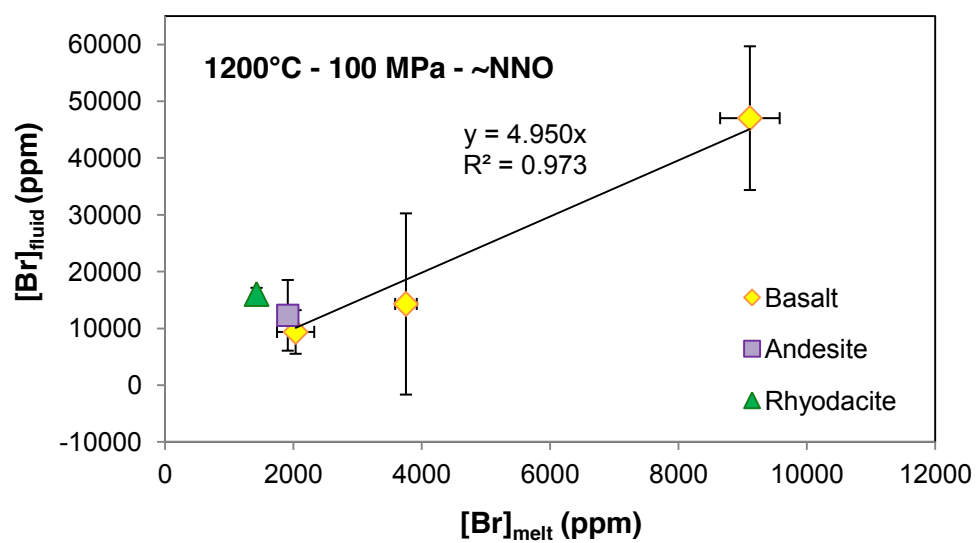
Table 3. Major element composition (wt%) of the partitioning experiment glassy products

Experiment #	Run product ID	<i>n</i>	SiO ₂	TiO ₂	Al ₂ O ₃	FeO _{tot}	MnO	MgO	CaO	Na ₂ O	K ₂ O	P ₂ O ₅	Original Sum
1	M1-B	1	48.47 (37)	1.77 (9)	16.79 (18)	10.07 (32)	0.17 (10)	5.83 (20)	10.83 (25)	3.51 (16)	1.98 (14)	0.59 (8)	94.11
		0											
2	M2-B	1	48.36 (29)	1.75 (9)	16.84 (15)	9.89 (30)	0.17 (9)	5.85 (17)	11.01 (31)	3.61 (12)	1.92 (21)	0.60 (9)	94.37
		0											
3	M3-B	7	48.96 (59)	1.65 (16)	17.05 (19)	9.12 (38)	0.17 (12)	6.15 (5)	10.82 (26)	3.60 (10)	2.07 (20)	0.40 (12)	95.01
"	M3-A	7	59.54 (30)	1.27 (14)	16.32 (20)	7.36 (29)	0.10 (8)	2.74 (6)	6.33 (14)	4.46 (8)	1.66 (7)	0.21 (15)	95.14
"	M3-RD	6	71.31 (30)	0.40 (6)	14.77 (18)	2.15 (15)	0.10 (12)	0.72 (3)	2.40 (8)	4.90 (9)	3.20 (10)	0.07 (6)	95.56
4	M4-A1	6	59.50 (33)	1.28 (14)	16.37 (13)	7.66 (41)	0.19 (8)	2.73 (9)	6.35 (6)	4.11 (9)	1.59 (6)	0.22 (12)	93.51
"	M4-A2	6	59.52 (38)	1.36 (17)	16.45 (28)	7.50 (39)	0.18 (9)	2.68 (8)	6.35 (9)	4.14 (11)	1.56 (7)	0.27 (15)	92.77
"	M4-A3	6	59.70 (43)	1.33 (18)	16.55 (10)	7.19 (22)	0.20 (14)	2.66 (5)	6.31 (11)	4.12 (5)	1.61 (10)	0.31 (18)	93.18
"	M4-A4	6	59.44 (54)	1.38 (11)	16.27 (18)	7.73 (19)	0.28 (9)	2.71 (5)	6.34 (14)	4.17 (9)	1.51 (5)	0.16 (20)	92.81
"	M4-RD1	6	71.77 (26)	0.51 (4)	14.85 (20)	2.18 (28)	0.14 (5)	0.69 (4)	2.47 (7)	4.41 (34)	2.88 (19)	0.10 (6)	92.93
"	M4-RD2	5	71.48 (73)	0.48 (9)	14.92 (5)	2.35 (12)	0.05 (5)	0.69 (4)	2.46 (7)	4.51 (7)	2.86 (13)	0.19 (10)	92.35
"	M4-RD3	6	71.49 (61)	0.46 (7)	15.05 (19)	2.28 (25)	0.08 (11)	0.66 (2)	2.45 (11)	4.64 (9)	2.83 (11)	0.05 (8)	92.40
"	M4-RD4	7	71.68 (37)	0.45 (8)	14.63 (22)	2.40 (21)	0.09 (7)	0.71 (4)	2.37 (6)	4.58 (10)	2.90 (10)	0.18 (9)	92.10
5	M5-RD1	8	71.56 (31)	0.49 (8)	14.49 (29)	2.88 (21)	0.06 (8)	0.71 (3)	2.34 (8)	4.35 (8)	3.01 (19)	0.11 (6)	91.79
"	M5-RD2	8	71.47 (39)	0.42 (10)	14.40 (21)	3.01 (30)	0.08 (8)	0.70 (5)	2.41 (11)	4.41 (8)	2.97 (12)	0.11 (10)	92.69
"	M5-RD3	9	71.50 (31)	0.46 (10)	14.39 (13)	2.96 (19)	0.07 (7)	0.72 (4)	2.37 (6)	4.45 (14)	3.00 (19)	0.09 (10)	92.37
"	M5-RD4	7	71.31 (52)	0.41 (11)	14.44 (22)	2.89 (20)	0.05 (6)	0.71 (4)	2.38 (9)	4.58 (9)	3.07 (17)	0.16 (5)	93.19

Major element analyses recalculated to 100%

n is the number of analyses per productNumbers in parentheses indicate one standard deviation of *n* analyses in terms of smallest units cited

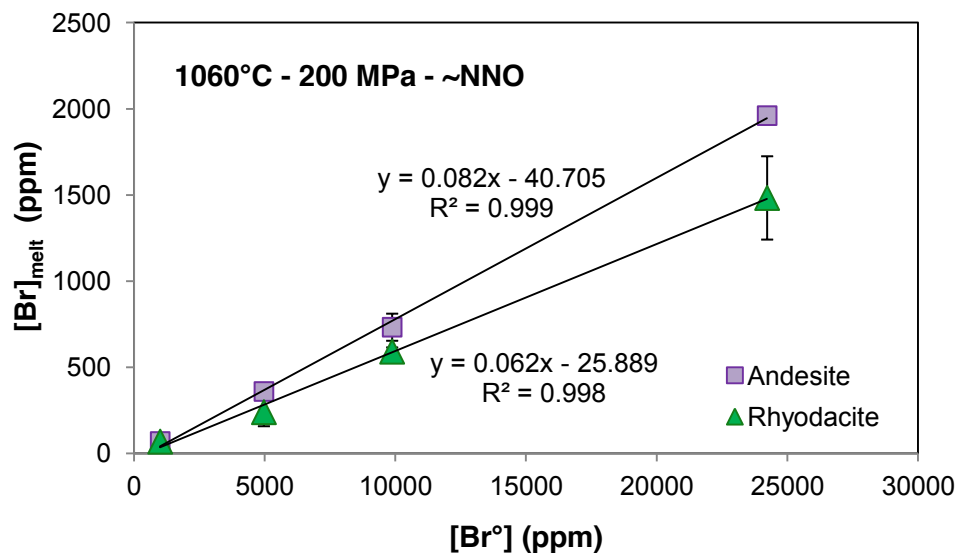
1277 **Figure 1**



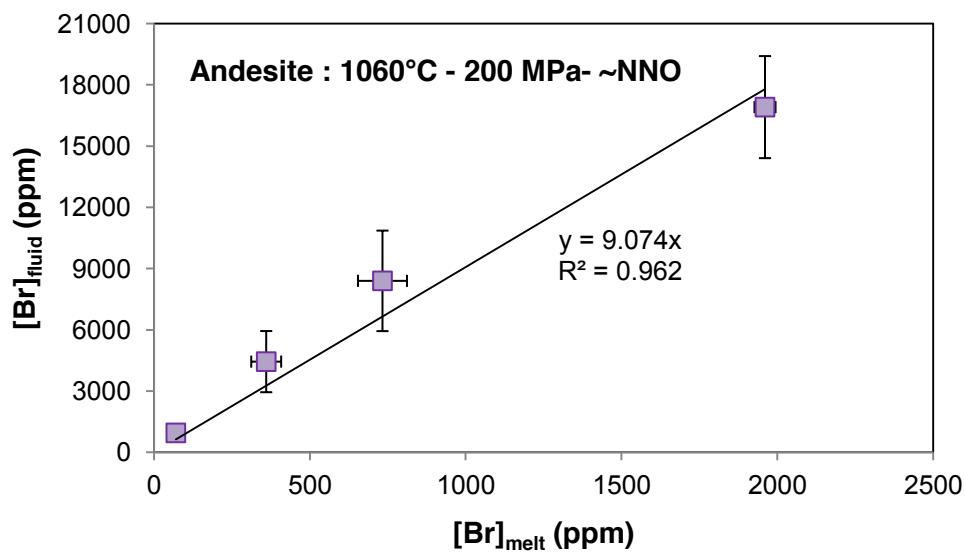
1278

1279

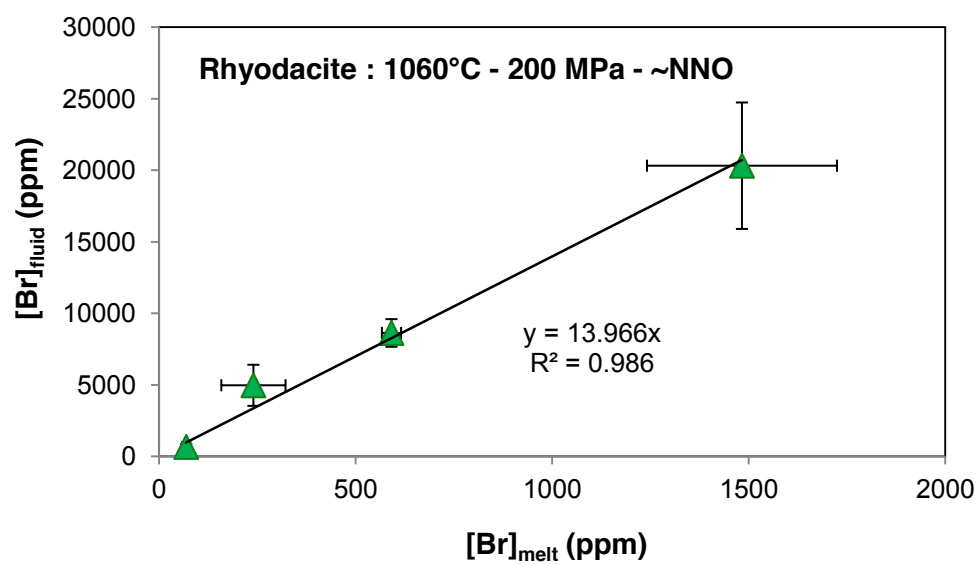
Figure 2 (a)



(b)



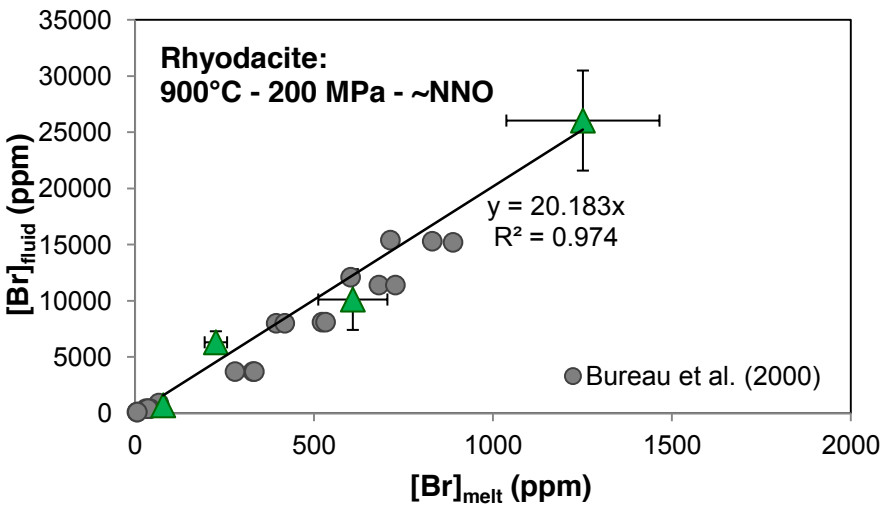
1289 (c)



1290

1291

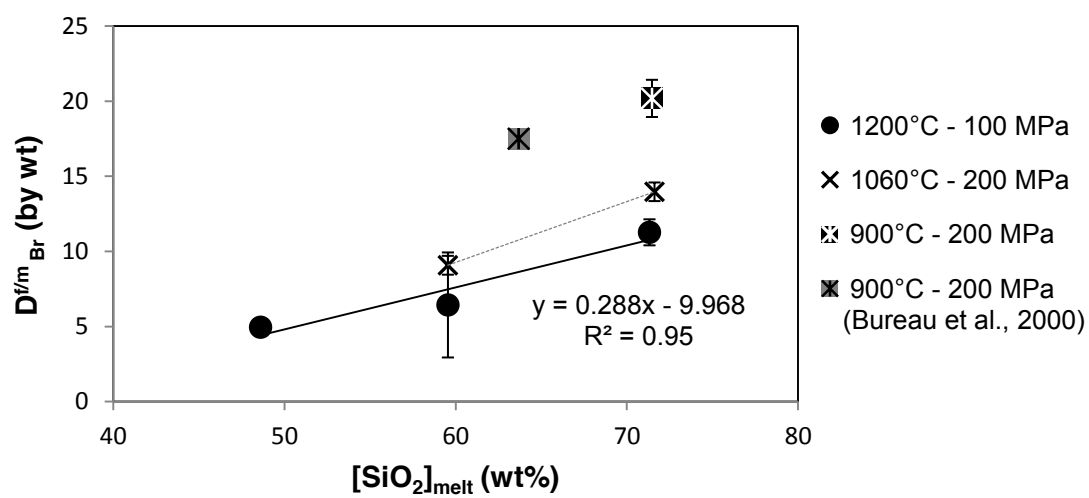
1292 **Figure 3**



1293

1294

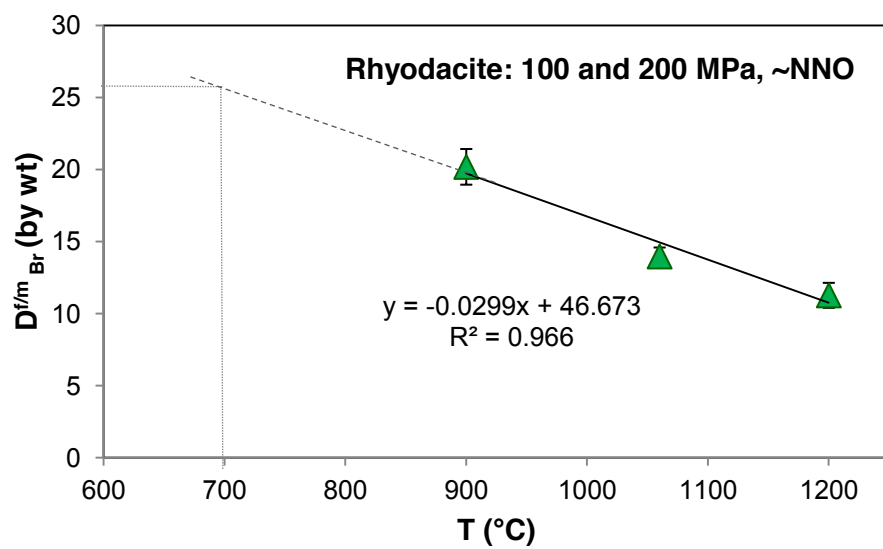
1295 **Figure 4**



1296

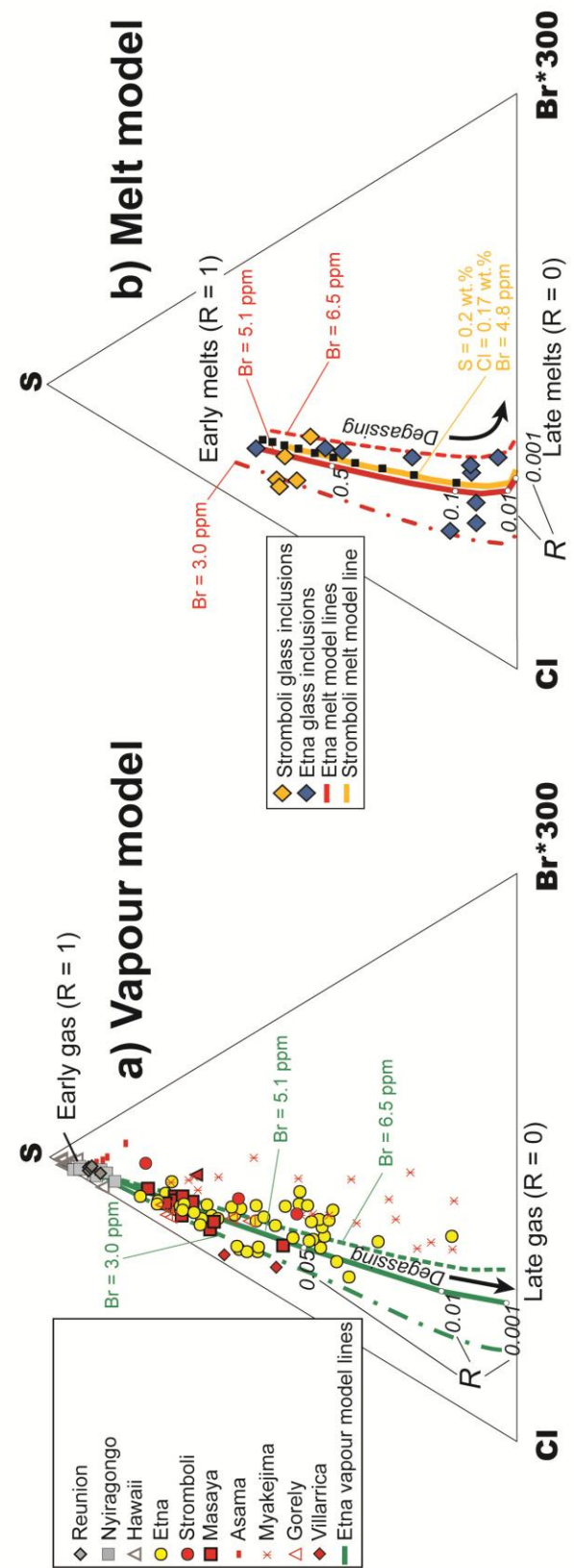
1297

1298 **Figure 5**



1299

1300



Supplementary material for online publication only

[Click here to download Supplementary material for online publication only: Figure A.1.pdf](#)

Supplementary material for online publication only

[Click here to download Supplementary material for online publication only: Supplementary Info_final.docx](#)